Energetics and Dynamics of Copper-coordinated Complexes Using Force Fields and Density Functional Theory

THESIS · MARCH 2016

DOI: 10.13140/RG.2.1.3036.3282

Niels Burzan
Empa - Swiss Federal Laboratories for Mate…

Thesis to get the degree of Master of Science in Nanoscience

Energetics and Dynamics of Cu-coordinated Complexes Using Force Fields and Density Functional Theory

Niels Burzan

21.12.2015

University of Basel
Natural Sciences Faculty
Institute of Physical Chemistry

Dean

Prof. Dr. Stefan Antusch

Referees

Prof. Dr. Markus Meuwly
Prof. Dr. Catherine Housecroft

...to boldly go where no man has gone before.

Contents

Abstract

This thesis investigates methods to compute the interactions, the transition metal copper exhibit in living systems and applied bio-inorganic technologies. Computational methods covered include classical force fields with special emphasis on transition metals as well as novel quantum mechanical calculations. Among the correct prediction of the geometry of copper(I) and copper(II) complexes is the thermodynamic and structural *trans* influence of ligands on the isomerization energy differences and bond length changes of square-planar copper(II) complexes. Furthermore, the structural properties and dynamics of copper(I/II)-imidazole complexes in water are investigated using VALBOND and DFTB3, both are shown to perform in good agreement with experiment. Also, a method to estimate the impact of oxidation of copper(I) on the complex geometry is investigated and accompanied by free energy calculations. Sophisticated understanding of the nature of molecules by high-performance computing has become possible at low costs nowadays and thus permits advanced *in silico* materials design.

1. Introduction

Copper in its ionized form, Cu^{1+} and Cu^{2+}, are very important metal ions for biological systems.[22, 33] For example, an integral part of photosynthesis is the electron transfer carried out by metallo-proteins like plastocyanine, shown in Figure 1.1. Due to the redox activity of copper it is a suitable co-factor for enzymatic catalysis. To possibly exploit this property for energy production copper is also investigated for solar energy approaches like dye sensitized solar cells and for biomimetic artificial photosynthesis, see Figure 1.3.[23] For medical aspects copper also plays an important role, e.g. in Alzheimer's disease: the dysregulation of copper is associated with oxidative stress and promoting the formation of amyloid plaques[10], see Figure 1.2. Therefore, effective computational methods to determine copper-complex dynamics and the atomistic relevance of a change in the redox-state are necessary. As depicted by the three examples, the geometrical arrangement of the ligands around the copper core is of crucial importance to simulate copper complexes. Several force fields already allow the computation of transition metals, focusing on the geometry of the complexes. Momec, developed by Comba *et al.*, is based on a purely ligand-ligand repulsion approach and is restricted to idealized and fixed geometries[7]. Shapes[1] and Valbond[9], both developed by Landis *et al.*, are both based on angular overlap consideration. Shapes employs a Fourier transform description of angular potentials whereas in contrast, Valbond predicts the equilibrium geometry using Pauling's strength functions for $sp^m d^n$ hybrids based on Valence Bond Theory. In this work, efforts to better assess the metal-protein interaction are presented by applying the Valbond-Trans[52] model to copper(II)-complexes. The *trans* influence extension of Valbond is beneficial if square planar complexes like copper(II) are to be investigated. Alongside that parametrization, the dynamics of an bioinorganic copper complex is investigated using a classical Charmm-Valbond force field and compared with a new quantum mechanical density functional tight binding 3^{rd} (DFTB3)[14] model mixed with Charmm, which was recently parametrized for copper.[16] DFTB3 is a quantum mechanical method faster than DFT B3YLP but still in good agreement with it.

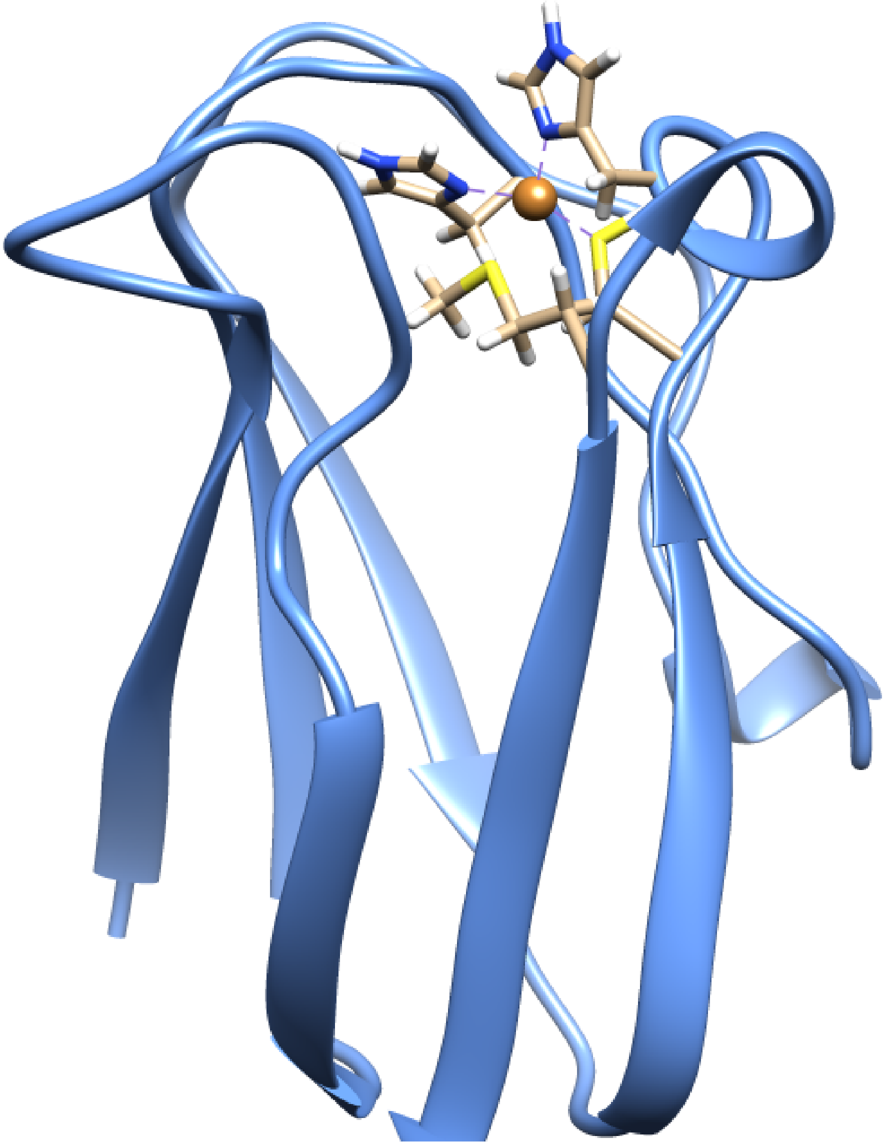

Figure 1.1.: The electron transfer protein plastocyanin contains as co-factor a copper ion. The coordination site consists of histidine, cystein and methionine, whereas the imidazole rings of histidine and cystein coordinate a copper ion by means of a trigonal planar structure. The nearby methionine, at 2.8 Å distance leads to a distorted trigonal pyramidal geometry which consequently destabilizes the copper(II) oxidation state and increases the redox potential of the whole protein. This illustrates the relation between coordination geometry and redox activity. Orange, the coordinated copper ion, light blue, the protein backbone, dark blue the nitrogen atoms of the imidazole ring of histidine, yellow sulfur atoms of cystein and methionine, beige the carbon atoms and in white the hydrogen atoms of the amino acids. The dotted lines refer to the trigonal planar geometry, formed by two histidine and one cystein residue coordinating a copper ion. Figure created with Chimera[47] of PDB entry 1BXU.[27]

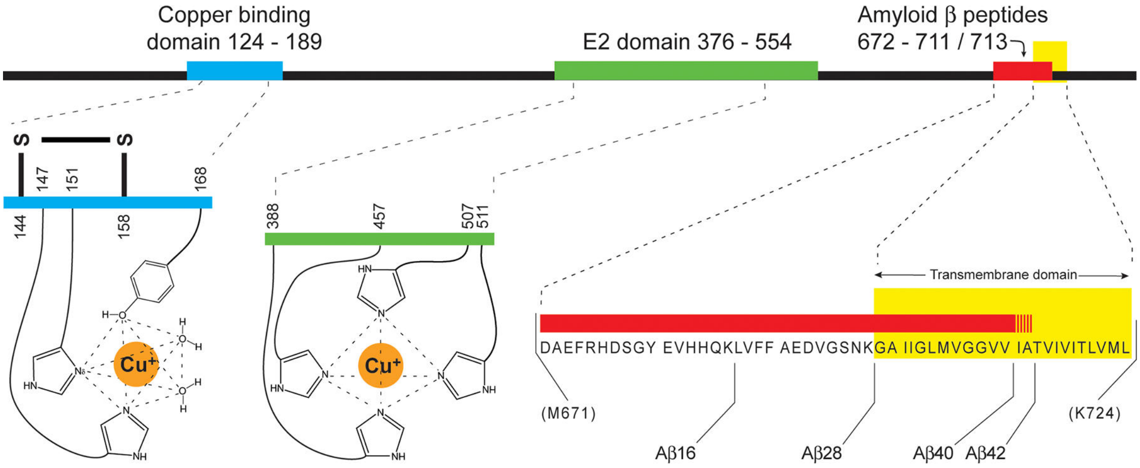

Figure 1.2.: Alzheimer's disease is linked to a dysregulation of copper ions, which are involved in the misfolding of amyloid proteins. The shown amyloid precursor protein (AAP, whole black strand) has 2 natural binding sites for copper (blue & green). Upon an interplay with other processes, the amyloid β peptides are cleaved from the APP and can exhibit multiple interactions with copper ions by means of square-planar complexes (at positions Aβ16, Aβ28, Aβ40, Aβ42). These interactions promote the formation of amyloid plaques which in turn give rise to a Alzheimer's disease like pathology. Figure taken from Eskici *et al.*[10]

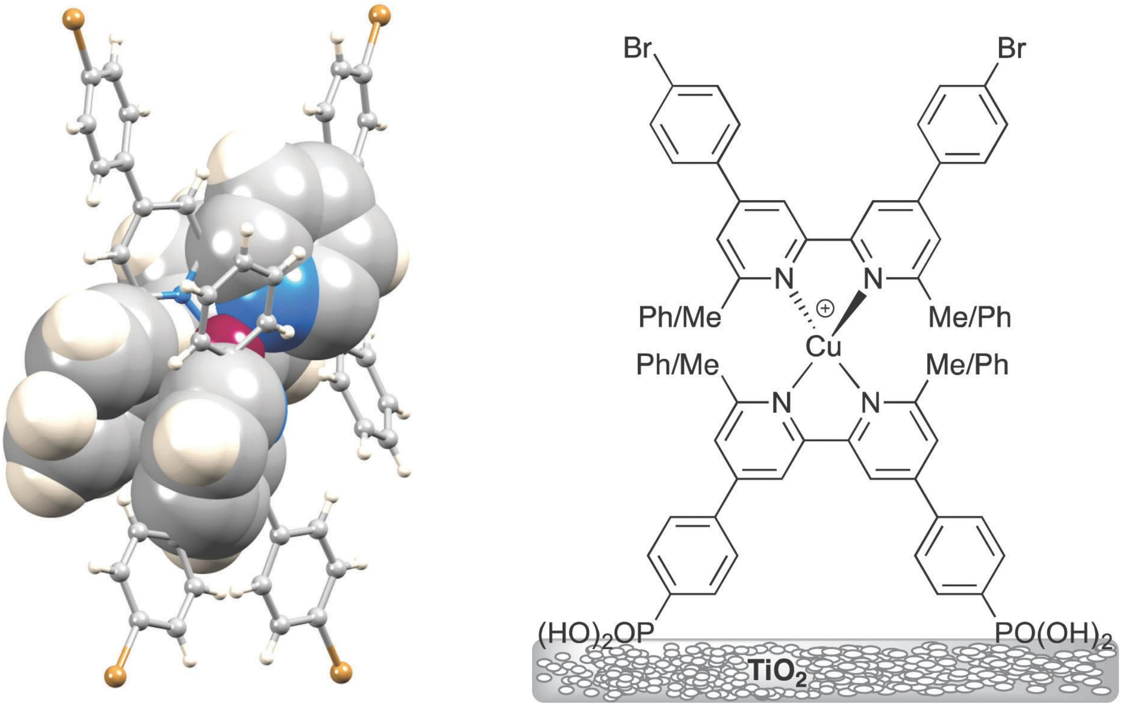

(a) (b)

Figure 1.3.: Redox activity of copper I/II complexes exploited in dye-sensitized solar cells: bio-inorganic dye molecules are capable photon absorbers, lifting the dye molecule to an excited state which results in electron ejection into the titanium-dioxide substrate (b), leaving the copper (I) oxidized to copper(II). This comes along with a geometrical change as Cu(I) it tetrahedral whereas Cu(II) is square-planar. The stability and performance of such systems can be enhanced by rendering the geometry. It is shown that the tetrahedral Cu(I) geometry can be flattened by substituting the methyl groups nearby the copper core with phenyl groups (b). The introduced two pairs of phenyl-pyridine rings exhibit a flattening by $\pi - \pi$ stacking (a). Figure taken from Housecroft and Constable[23].

2. Theory

2.1. Overview

This chapter summarizes the theoretical basics of the models used in this study. In section 2.2, the idea of the potential energy surface as the most intuitive model of the nature of chemicals is introduced. From section 2.3 on, the most important approaches to model a chemical structure are presented one by one. Thereafter, section 2.9 introduces the valence bond theory, which is the foundation for the force field studied in this work. Its formalism is presented in section 2.10.

2.2. Computational chemistry

Computational chemistry is motivated by the ambition of prediction. Knowledge gained by measurement can be used to successfully predict observables under related conditions. First of all, computational chemistry is about the structure of molecules which are the building blocks of materials. The simplest description of a molecule is the molecular formula. This provides limited information of the atoms the molecule is composed of and their relative position in space. From the latter, one can gain insight into the connectivity of the molecules atoms. Finding the coordinates which lead to a energy minimum, hopefully the absolute minimum of the molecule, is one essential task of the computational chemist. Yet reality is different: thermal fluctuation, stereoisomerism, tautomerism, etc. making any lab measurement an average over a very large equilibrium mixture of the substance of interest. To better address the reality respectively experiment, one should consider all possible structures. Using the Born-Oppenheimer approximation[5], the potential energy surface (PES) of a given structure can be characterized. For a molecule with $N \geq 3$ atoms, the PES has $3N-6$ coordinate dimensions. In other words, the hyper-surface spanned by the potential energy of all possible atomic arrangements within the molecule, is resulting in the PES. For a visualization of the PES, one has to reduce the dimensionality, e.g. by setting one atom as the origin of a coordinate system and describe all other relative to that using internal coordinates. Thus, several bond lengths, valence angles and dihedral angles with respect to the origin can be constructed. Local minima of the PES correspond to stable molecular structures. Saddlepoints, which are defined by downward curvature in only one but upward curvature in all other directions, connecting two local minima, correspond to transition states. These features of a

PES allow for computation of possible structures and determination of potential energy barriers. Furthermore, thermodynamic quantities like the free energy, enthalpy as well as equilibrium constants and rate constants can be computed from the observed energetic differences between the minima and the connecting transition state structure from the PES.[8]

2.3. The chemical bond

The modeling of bonds is a fundamental part of computational chemistry. Bond stretching potential energy can be derived from spectroscopic data. Consider a heterodiatomic molecule consisting of atom A and B, connected by a bond $r_{equilibrium}$ which leads to a minimum in the potential energy. The potential energy of such a system at any point can be found by exploiting a Taylor expansion over $r_{equilibrium}$

$$U(r) = U(r_{eq}) + \left.\frac{dU}{dr}\right|_{r=r_{eq}} (r-r_{eq}) + \frac{1}{2!}\left.\frac{d^2U}{dr^2}\right|_{r=r_{eq}} (r-r_{eq})^2 + \frac{1}{3!}\left.\frac{d^3U}{dr^3}\right|_{r=r_{eq}} (r-r_{eq})^3 + \cdots \tag{2.1}$$

By definition, the energy at the equilibrium bond length $U(r_{eq}) = 0$ and $r_{equilibrium}$ is the minimum point which means that the second term becomes also zero. For the calculations presented in this work, where the bond length are only slightly perturbed from $r_{equilibrium}$, the Taylor expansion can be truncated after the quadratic term. Replacing the second derivative of the potential energy with the constant k, the vibrational potential energy reads

$$U\left(r_{AB}\right) = \frac{1}{2} k_{AB} \left(r_{AB} - r_{AB,eq}\right)^2 \tag{2.2}$$

This is analog to Hooke's law where k_{AB} is interpreted as the force constant of a spring connecting atoms A and B with a disturbance of the bond length around the equilibrium length. As long as no big deviations from the minimum bond length are investigated, one should use this equation. Otherwise, the in terms of computation more expensive Morse function should used to model the bond potential

$$U\left(r_{AB}\right) = D_{AB}\left[1 - \exp\left\{-\alpha_{AB}\left(r_{AB} - r_{AB,eq}\right)\right\}\right] \tag{2.3}$$

With D_{AB} the dissociation energy of the AB-bond and α_{AB} as a fitting constant. The Morse function reproduces the potential energy curve quite well and also allows for a bond breaking. Therefore it is considered closer to the reality than the simple harmonic model.[8]

2.4. The angle between bonds

Similarly, for a simple, purely classical model, the angle Θ between atoms A,B and C respectively between the bonds AB and BC can be derived from a Taylor expansion as

$$U\left(\Theta_{ABC}\right) = \frac{1}{2}\left[k_{ABC} + k^{(3)}_{ABC}\left(\Theta_{ABC} - \Theta_{ABC,eq}\right) + k^{(4)}_{ABC}\left(\Theta_{ABC} - \Theta_{ABC,eq}\right)^2 + \cdots\right] \cdot \left(\Theta_{ABC} - \Theta_{ABC,eq}\right)^2 \quad (2.4)$$

or simplified, as a harmonic potential

$$U\left(\Theta_{ABC}\right) = \frac{1}{2}k_{ABC}\left(\Theta_{ABC} - \Theta_{ABC,eq}\right)^2 \quad (2.5)$$

Both expressions are quite limiting, e.g. for linear bond angles with $\Theta = \pi$. In Addition, for inorganic systems, this equations do not replicate the appearance of multiple equilibrium values. Therefore, an alternative description for the angle will be discussed vide infra.[8]

2.5. The dihedral between four atoms

Torsion angles between four atoms A, B, C and D are specified by the angle between AB- and CD-bonds as if they were projected into a plane bisecting the BC-bond. As a convention, clockwise rotation of the bond in front of that plane leads to positive values for the dihedral ϕ.

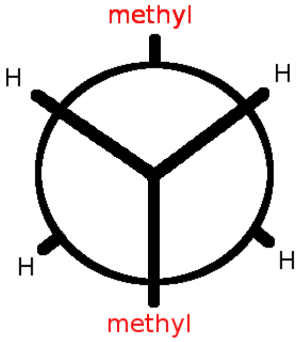

Figure 2.1.: Example of antiperiplanar arrangement of two methyl groups (Newman projection). Antiperiplanarity is often associated with minima of the dihedral energy.

$$U\left(\phi_{ABCD}\right) = \frac{1}{2}\sum_{\{j\}_{ABCD}} V_{j,ABCD}\left[1 + (-1)^{j+1}\cos\left(j\phi_{ABCD} + \psi_{j,ABCD}\right)\right] \quad (2.6)$$

Another convention, $-\pi < \phi \leq \pi$, is introduced to account for the observation, that many dihedrals are at minimum energy for antiperiplanar arrangements, i.e. if $\phi = \pi$, see Figure 2.1. For periodicity of the torsion angle is accounted by the representation of an expansion of periodic functions as a Fourier series. V_j is the term amplitude and the periodicities are described by j. If $\phi = \pi$ and the phase angle $\psi = 0$ the sum equals zero due to the $(-1)^{j+1}$part. Thus the torsional energy for antiperiplanar geometries is minimized. [8]

2.6. The van-der-Waals interaction

Two not interacting atoms (e.g. noble gases) approaching each other are classically supposed to experience only one force - an infinitely strong repulsion if their separation r reaches twice the radius of each atom r_{VdW}, as represented in Figure 2.2. However, quantum mechanics revealed, that the electronic wave functions of atoms are correlated and they simultaneously can develop orientated electrical moments. The arising induced dipole - induced dipole interaction is attractive. This force is known as London or dispersion force[42] and the resulting potential scales inverse on the distance between the atoms: $U\left(r_{AB}\right) \sim -\frac{1}{r_{AB}^6}$

Still, for decreasing bond lengths, the electron densities interpenetrate the close neighboring atom which causes the Pauli repulsion. As long as there is no possibility for bonding, the energy of the system skyrockets.

The combination of repulsion and dispersion energies leads to the famous Lennard-Jones potential[30]

$$U\left(r_{AB}\right) = \frac{a_{AB}}{r_{AB}^{12}} - \frac{b_{AB}}{r_{AB}^{6}} \tag{2.7}$$

with a and b being constants specific to the atom type of A and B. The dependence of the repulsive term, $\frac{1}{r_{AV}^{12}}$ is used due to the ease of calculation which performs faster than a better fitting exponential dependence, especially if one considers the vast amount of non-bonded calculations which have to be evaluated. In a system consisting of N atoms, N^2 of such interactions occur. Another form of the Lennard-Jones potential evokes other insights

$$U\left(r_{AB}\right) = 4\varepsilon_{AB}\left[\left(\frac{\sigma_{AB}}{r_{AB}}\right)^{12} - \left(\frac{\sigma_{AB}}{r_{AB}}\right)^{6}\right] \tag{2.8}$$

with ε_{AB} the potential well depth and σ_{AB} the separation length between atoms A and B, at which the repulsive and attractive forces are equal, i.e. the potential $U = 0$. Differentiation followed by setting zero shows where the potential minimum lies

$$\frac{dU\left(r_{AB}\right)}{dr_{AB}} = \frac{4\varepsilon_{AB}}{r_{AB}}\left[-12\left(\frac{\sigma_{AB}}{r_{AB}}\right)^{12} + 6\left(\frac{\sigma_{AB}}{r_{AB}}\right)^{6}\right] \tag{2.9}$$

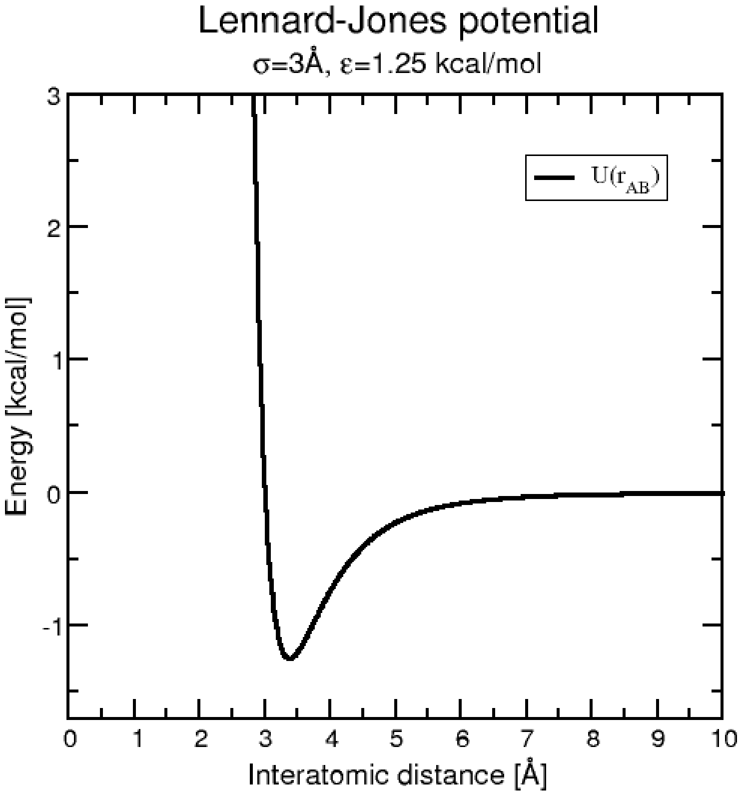

Figure 2.2.: Lennard-Jones potential[30] to model the non-bonded interaction. For the plot, a rather large σ of 3Å and an ϵ of 1.25 $^{kcal}/_{mol}$ were used.

Setting equation (9) to zero reveals the bond length at the minimum potential $\tilde{r}_{AB} = 2^{1/6}\sigma_{AB}$. Evaluation of that bond length in equation (8) leads to the potential $U = -\varepsilon_{AB}$ indicating the potential well depth.[8]

2.7. Electrostatics

In order to be able to compute other elements than noble gases like ions, one has to consider the interactions of permanent electric moments. By assignment of partial charges to each atom the electrostatic interaction can easily modeled by Coulomb's law for two separated point charges

$$U_{AB} = \frac{q_A q_B}{\epsilon_{AB} r_{AB}} \tag{2.10}$$

with $q_{A/B}$ the partial charge of atom A respectively B, r_{AB} the separation distance, $\epsilon_{AB} = \epsilon_0 \epsilon$ the permittivity of the substance between the charged atoms A and B (composed of the free space permittivity $\epsilon_0 = 8.854187817 \cdot 10^{-12}\,^{F}/_{m}$ and the material specific and dimensionless relative permittivity ϵ).[8]

2.8. Parametrization

Because force fields are a collection of functions and associated constants, the parametrization of force fields is an important task to reproduce experimental measurements as good as possible. The experimental data for molecular mechanics consists of structural, energetic and molecular electric moments, if at hand. The experimental data is often supplemented by *ab inito* data, i.e. from higher level calculations. The goal is, to find the force field parameters in such a way, that a function of the deviation of predicted against measured observables is minimized.

2.9. Valence bond theory

Valence bond (VB) theory roots back to Lewis paper[38] The Atom and The Molecule, introducing the notion of electron pair bonding and the famous octet rule in 1916. This theory was supported by Heitler and London's work Interaction Between Neutral Atoms and Homopolar Binding[20], which explained the bonding of non-ionic elements with quantum mechanics. Later on, Pauling and Slater generalized and combined both concepts and extended it for polyatomic molecules.[44]

In VB theory, the energy of a covalent bond is governed by the energy of resonance between two atoms. Consider the formation of the H_2 molecule, by bringing two hydrogen atoms with each one electron close together. As long as they are far away one can distinguish between atoms $H_A\left(\alpha\right)$ and $H_B\left(\beta\right)$ having electrons α and β respectively, leading to the wave function ψ_1. Upon formation of a molecule, the electron of each hydrogen atoms is shared with the partner atom. Another wave function ψ_2 is possible, if the electrons are exchanged, i.e. $H_A\left(\beta\right)$ and $H_B\left(\alpha\right)$. Since they are indistinguishable, the description leads to a superposition formulated as a linear combination $\psi_{bond} = \lambda_1\psi_1 + \lambda_2\psi_2$ with a normalization factor $N = \frac{1}{\sqrt{\lambda_1^2+\lambda_2^2}}$. If the electrons α and β are spin paired, a constructive interference leads to the bond formation denoted as $\psi_+ = N\left(\psi_1 + \psi_2\right)$, if the spin's are parallel the wave function reads $\psi_- = N\left(\psi_1 - \psi_2\right)$ which is antibonding.

In this model, for ψ_+ the separation length of the nuclei is overestimated compared to experimental values, i.e. predicted 87 pm vs. measured 74 pm, and underestimates the H-H bond dissociation energy, i.e. $\Delta U_{prediction} = 303\,\frac{kJ}{mol}$ vs. $\Delta U_{experiment} = 458\,\frac{kJ}{mol}$. To overcome that, VB theory allows to relocate the two electrons over the two centers, forming ionic species: anionic $H_A\left(\alpha,\beta\right)$ and cationic H_B and vice versa, giving rise to the wave functions ψ_3 and ψ_4. Since H_2 is a homonuclear diatomic, the probability of ψ_1 and ψ_2 are equal as are ψ_3 and ψ_4. The bond forming linear combination thus reads $\psi_+ = N\left[\left(\psi_1 + \psi_2\right) + c\left(\psi_3 + \psi_4\right)\right]$. If one chooses the constant c≃0.25, the predicted values for the separation length and bond dissociation energy are within good agreement with the measurements. This leads to the conclusion that the single bond in hydrogen has 75% covalent and 25% ionic character. The total electronic wave function can be simplified to:[24]

$$\psi = N\left[\psi_{covalent} + (c \cdot \psi_{ionic})\right] \tag{2.11}$$

The covalent bond can further be investigated and the bond strength and angles can be estimated. For this purpose, one should consider orbital wave functions of two close atoms, which start to overlap, i.e. interpenetrating the bond-electron distribution of them. For example Pauling states that the bond strength and direction is associated with the degree of overlap and dominated by the partner which can overlap more than the other partner. Hence only stable atomic orbitals can form stable bonds, the direction in which a bond lies, is given by the angular distribution of the used atomic orbital. A spherically symmetrical s-orbital can form one bond in any direction whereas the 3 p-orbitals are restricted to the cartesian axis, in which they lie (p_x,p_y,p_z). Due to the reduced volume occupied by p-orbitals, their wave magnitude is $\sqrt{3}$ times higher than that of the same shell s-orbital, for which reason p-orbitals form stronger bonds than s-orbitals. It was shown that the bond energy is proportional to the magnitude-product of the bond-forming orbitals, thus the energy of an s-p bond is $\sqrt{3}$ times as high as that of an s-s bond and consequently a p-p bond is 3 times stronger.

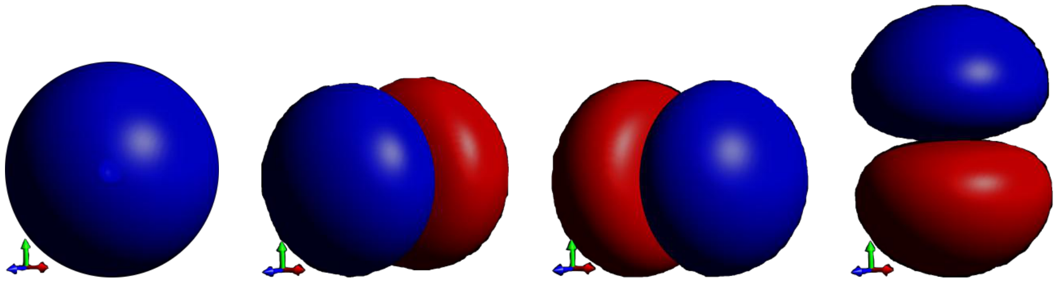

Figure 2.3.: Illustrations of 2s, $2p_x$, $2p_y$ and $2p_z$ orbitals of carbon, generated with Avogadro[18]

The formation of hybrid bond orbitals, which give rise to the tetrahedral molecular geometry, can also be described on the basis of VB theory for the example of carbon. Instead of forming three p-orbital originating bonds with strength $\sqrt{3}$ along the three axis and one s-orbital originating bond of strength 1 in any direction, all 4 outer shell orbitals of carbon merge together, creating sp-hybrid orbitals. The reason lies in the minimization of the systems energy by maximization of the bond energy: linear combination of s- and p-orbitals leads to a bond strength of 2 which is also strongly directed. All four sp-hybrid orbitals pointing towards a corner of a regular tetrahedron, with angles of 109 degree between them. Because the bond strength is based on the angular distribution of a bond orbital, one can show the lowered energy for sp-hybrid orbitals. Assume, the wave function ψ_s and ψ_{p_x}, ψ_{p_y}, ψ_{p_z}, at

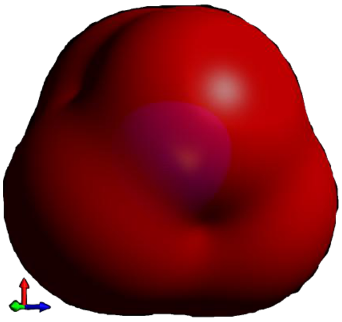

Figure 2.4.: Illustration of the four resulting 2sp^3 orbitals of methane, generated with Avogadro[18]

which their radial part can be neglected and they differ only in their angular part

$$\begin{cases} s &= 1 \\ p_x &= \sqrt{3}\,\sin\Theta\,\cos\Phi \\ p_y &= \sqrt{3}\,\sin\Theta\,\sin\Phi \\ p_z &= \sqrt{3}\,\cos\Theta \end{cases} \tag{2.12}$$

with Θ and Φ the angles used for polar coordinates. All four functions are normalized to 4π using $\int_0^{2\pi}\int_0^{\pi} f^2 \sin\Theta\, d\Theta\, d\Phi$. Furthermore, the four functions are orthogonal, i.e. the normalized integral of the product of two of them equals zero. Screening for a function which leads to a larger bond strength than $\sqrt{3}$ of pure p-orbitals using

$$f = as + bp_x + cp_y + dp_z \tag{2.13}$$

By also requiring normalization to function f, i.e. $(a^2 + b^2 + c^2 + d^2) = 1$, one can determine the bond strength of an sp-orbital. For one direction, e.g. the z-axis: $f_1 = as + dp_z = as + \sqrt{1-a^2} \cdot p_z$, By substituting s and p_z from Equation 2.12 and setting the bond direction $\Theta = 0$, $f_1\left(\Theta = 0\right) = a + \sqrt{3\left(1-a^2\right)}$. Finding the maximum by differentiating (with respect to a), a=$\frac{1}{2}$ and f_1 as the best bond orbital in z-direction

$$f_1 = \frac{1}{2}s + \frac{\sqrt{3}}{2}p_z = \frac{1}{2} + \frac{3}{2}\cos\Theta \tag{2.14}$$

Hence the strength of an sp-orbital in z-direction, $\Theta = 0$ and $\cos\left(\Theta\right) = 1$, equals 2. The same holds true for the 3 remaining directions due to the orthogonally. All four best sp-hybrids have strength 2 and are separated by 109 degree angles while being at the energetic minimum.[50, 45]

2.10. The Valbond and Valbond-Trans force field

The overlap of hybrid orbitals between bonding partners is used in the VALBOND[9, 51, 34, 35, 11] force field to capture a ligand-metal-ligand bond arrangement. As shown above, angular distortions determine the shape of molecules. VALBOND is used to find the correct bending potentials of these distortions and therefore predict the molecular geometry. It can be used for non-hypervalent and hypervalent molecules, which do not follow the octet rule.[51] Furthermore, it was implemented to evaluate transition metal complexes.[34, 11] The formulation corresponds basically to the one shown before but for clarity the generalized hybrid orbital strength functions are given for two equivalent sp^3 hybrid orbitals: $\phi_1 = \frac{1}{2}\left(|1s\rangle + \sqrt{3}\,|p_z\rangle\right)$ and $\phi_2 = \frac{1}{2}\left[|1s\rangle + \sqrt{3}\left(\cos\alpha\,|p_z\rangle + \sin\alpha\,|p_x\rangle\right)\right]$, where φ_1 is maximal along the z-axis and φ_2 in the xz-plane, forming the angle α with φ_1. As shown in section 2.9, their strength S is given by the angular orientation and leads in both cases to $S = 2$. The overlap between both sp^3 hybrid orbitals results in $\Delta = \frac{1}{4}\left(1 + \sqrt{3}\cos\alpha\right)$. S depends on the magnitude of the overlap and the decrease of the strength can therefore related to the extend of the overlap and thus indicates the electron density in the bond forming region.

The main advantage of the VALBOND force field is the correct prediction of the angular parts, especially for transition metals. Always, VALBOND is mixed with other force fields like CHARMM. The additional term for selected atom types is for each ligand i

$$U_i = k_i\left[S_i^{max} - S_i\left(\alpha_{i,j}\right)\right] \tag{2.15}$$

with k_i an force constant, S_i^{max} the maximum strength of the hybrid orbital, $S\left(\alpha_{i,j}\right)$ the reduction of the maximal strength due to the angular orientation of the involved hybrid orbitals of two different ligands i and j.[25] Strength represents in this term the density of electrons in the bond forming region. The maximum strength of a particular sp^{m}d^n hybrid orbital is given by

$$S^{max} = \sqrt{\frac{1}{1+m+n}}\left(1 + \sqrt{3m} + \sqrt{5n}\right) \tag{2.16}$$

whereas the reduction of the maximal strength due to angular distortions can be determined by

$$S\left(\alpha\right) = S^{max}\sqrt{1 - \frac{1 - \sqrt{1 - \Delta^2}}{2}} \tag{2.17}$$

which depend on on the angular overlap Δ of two sp^{m}d^n hybrid orbitals, which reads

$$\Delta = \frac{1}{1+m+n}\left(|1s\rangle + m\,\cos\alpha\,|p_z\rangle + \frac{n}{2}\left(3\cos^2\alpha - 1\right)|d_{z^2}\rangle\right) \tag{2.18}$$

In case of hypervalent molecules, where several resonance structures are possible, the geometry's has to be described by a weighting factor c_j. The total energy of a 3-center/4-electron bond (e.g. in ClF_3) is the sum of three resonance structures, whereas each of them is a mixed ionic-covalent Lewis structure as explained in the beginning of section 2.9 by the example of the hydrogen molecule. Consider CF_3, assigning a bond order of 1 to one particular bond leaves the other CF bonds with the bond order $1/2$, and, due to the possible resonance structure, the according cyclic permutation of the bond orders. The total energy of the CF_3 molecule is given by $U_{tot} = \sum_{j=1}^{3} c_j E_j$ with the weighting factor c_j which depends on the geometry of the molecule. These also called mixing coefficients can be chosen as

$$c_j = \frac{\Pi_{i=1}^{hype} \cos^2 \alpha_i}{\sum_{j-i}^{config} \Pi_{i=1}^{hype} \cos^2 \alpha_i} \tag{2.19}$$

The products run over all hypervalent angles i, config, the number of possible resonance configurations. Generalized, the total energy of hypervalent molecules reads for all possible resonance configurations N

$$U_{tot} = \sum_{j=1}^{N} c_j E_j \tag{2.20}$$

The energy for each resonance structure $E\left(\alpha\right)$ can be calculated by

$$E\left(\alpha\right) = BOF \cdot k_\alpha \left(1 - \Delta\left(\alpha + \pi\right)^2\right) \tag{2.21}$$

introducing the bond order factor (BOF), k_α the VALBOND parameter for hypervalent molecules (k for nonhypervalent ones), Δ the bond overlap of $sp^m d^n$ hybrid orbitals as shown in Equation 2.18 and α the bond angle. The BOF is obtained by multiplication of the two formal bond orders of the bonds specified by the hybrid orbitals (with angle α between them).[25]

The further development of the VALBOND force field comprised the consideration of the *trans* influence,[52] which is especially pronounced in planar complex geometries, e.g. in Pt(II) or Cu(II) as well as in octahedral complexes. In the ground state of a molecule, a geometry L1-M-L2, where L1 is a ligand *trans* to a different ligand L2, both bound to a metal core M, a thermodynamic and a structural *trans* influence is expected[32]. Because of the presence of L2, the L1-M bond is weakened, depending on the chemical identities of L1 and L2 (thermodynamic *trans* influence). The same dependence is observed for the structural *trans* influence, which reports changes in the bond length between L1 and M.[2] The VALBOND hypervalent related Equation 2.21, i.e. for the 3-center/4-electron bond,

$$L1 : M - L2 \leftrightarrow L1 - M : L2$$

shows the the bending energy as a 180 degree shifted overlap between two orbitals and thus, linear geometries are favored in hypervalent bonds (i.e. there is minimum for $\alpha = \pi$). Reweighing the energy dependence on the chemical identity of the ligands L1 and L2 trans to each other in the L1-M-L2 motif leads to

$$U_{trans} = \sum_{trans} p_{AB} \left[\Delta \left(\alpha + \pi \right) \right] \tag{2.22}$$

A and B are the atoms of L1 and L2 bonded to the metal M, p_{AB} is the parameter of the thermodynamic *trans* influence and depends on the atom types A, B and M, α is the L1-M-L2 angle. Applying the linearity ($\alpha = \pi$) it follows $\Delta \left(\alpha + \pi \right) = 1$ which simplifies the *trans* influence energy expression to

$$U_{trans} = \sum_{trans} p_{AB} \tag{2.23}$$

The influence of the bond length, i.e. the structural *trans* effect, can be determined by

$$r_{A(B)} = r_A^0 \left(1 + s_A + \Delta \left(\alpha + \pi \right)^2 \cdot \frac{i_B}{100} \right) \tag{2.24}$$

with $r_{A(B)}$ the M-A bond length, rendered by atom type B *trans* to A. r_A^0 is the unperturbed bond length, s_A the bond lengthening sensitivity of atom type A, i_B the bond lengthening intensity of atom type B. Again, for hypervalent bonds hold $\Delta \left(\alpha + \pi \right) = 1$ which simplifies the equation for the structural *trans* influence[25]

$$r_{A(B)} = r_A^0 \left(1 + s_A \cdot \frac{i_B}{100} \right) \tag{2.25}$$

The effect, in which a ligand forming the stronger bond while weaken the bond between another ligand and the metal, is found favor, is called *antisymbiosis*. That means, stronger ligands tends to preferentially bind *trans* to weaker ligands, and vice versa.[52] The presented VALBOND formalisim will be used to study the dynamics of copper(I/II)-imidazole$_4$. The *trans* influence extension of VALBOND will be applied to copper(II) square planar structures to further extend the VALBOND-TRANS model.

3. Methods

3.1. Overview

In chapter 3 the methods are presented in more detail. First, section 3.2 and section 3.3 describe how two classical force fields are combined to offer the possibility to study transition metal including organometallic compounds. To compare the results, two quantum mechanical based calculation methods are used, which are presented in section 3.4 and section 3.5. The basic approach for the expansion of the VALBOND-TRANS force field for square-planar copper(II) complexes is presented in section 3.6. Furthermore, free energy calculation of the copper(I) ion oxidation to copper(II) is shown in section 3.7

3.2. Charmm-Valbond

CHARMM is a widely used molecular mechanics force field for biomolecular chemistry.[6] It solves Newton's equation of motion $m\frac{\partial^2 x}{\partial t^2} = F = -\frac{dU}{dx}$, where U is called the force field. In summary, a force field describes the interaction of particles and consists of the following terms.

$$U = U_{bond} + U_{angle} + U_{Urey-Bradley} + U_{dihedral} + U_{improper} + U_{CMAP} + U_{electrostatics} + U_{van-der-Waals} \tag{3.1}$$

These are the terms for the forces of bonded particles and, the last two terms, for non-bonded particles. Term called Urey-Bradley is needed for obtaining vibrational spectra, the improper term to remain chirality and planarity and thus support the dihedral term, the CMAP term is used to treat conformational properties of protein backbones - since these three are not of interest for this work, they are not further mentioned. All others terms are explained in the theory part, see chapter 2. To calculate a many particle system, it is necessary to sum up the bonded terms (bond, angle, dihedral) over all involved, i.e. bonded, atoms. The nonbonded terms (electrostatics, van-der-Waals) are added together over all interacting pairs. The standard CHARMM was mixed with the VALBOND force field to countervail for the poor prediction performance if organometallic substances are simulated. Therefore, the determination of the angle imidazole-copper-imidazole is calculated by VALBOND whereas the rest of the system is simulated using the CHARMM force field.

3.3. Copper(I/II)-Imidazole Charmm input file with Valbond

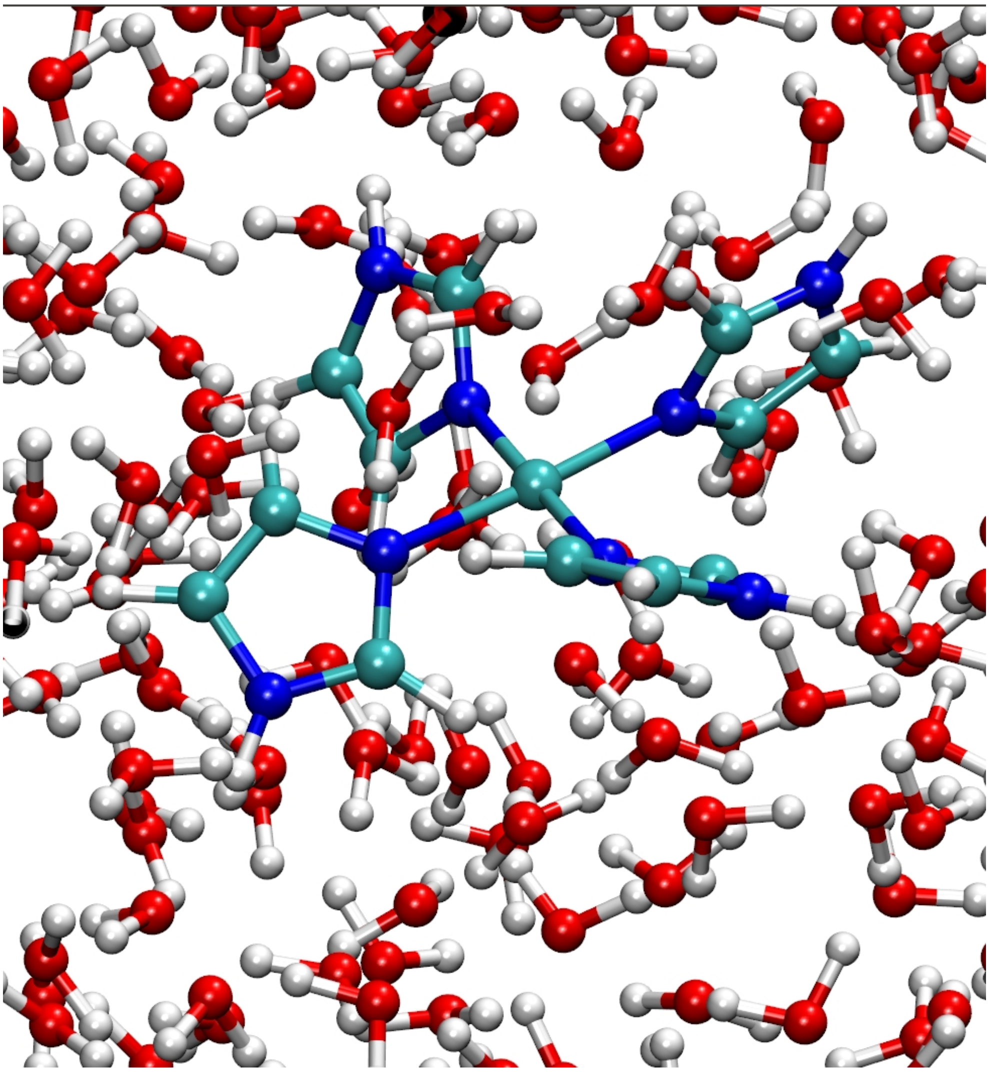

Figure 3.1.: Copper(II)-imidazole within a cubic box with 30 Å edge length and periodic boundary conditions. The solvent is simulated by using 584 TIP3P water molecules models. Figure generated using VMD[26].

A standard CHARMM input file was adapted for our purpose in the following way. First, the topology, parameter, psf and coordinate files are read in. The topology file defines the copper (I) - and copper (II) - Imidazole complexes with different partial and total charges. The partial charges were derived from B3LYP 6-31(d,p) DFT calculations in GAUSSIAN using either Mulliken or natural bond orbital (NBO) charges. The parameter file from CHARMM version 27 for proteins and nuclei acids was used, as it contains all necessary parameters. The sections counting the imidazole atom types, with parameters fitted for histidine, were silenced, whereas the imidazole-only parts were activated. This is of importance due to the fact that the imidazole ring is part of the amino acid histitide, as shown in Figure 1.1. The psf and coordinate files were generated using Charmm by combination of a pdb-file containing an optimized structure of copper(I/II)-Imidazole and a pdb-file containing a cubic box TIP3P[31] water molecules with edge length of 30 Å. Water molecules which ended up after the combination within a radius of 3 Å of the copper(I/II)-imidazole, were deleted. Furthermore, due to the different geometry depending on the oxidation state, additionally 3 random chosen water molecules have been deleted in the square-planar copper(II)-imidazole containing system to achieve 2 identically systems with the exception of the copper-complex. In total, the solvated copper(I/II)-imidazole systems consists of 2608 atoms of which 37 from the copper(I/II) complex and the remaining atoms represent 584 TIP3P water molecule models in a cubic box of volume 27 nm^3 with periodic boundary conditions. Water molecules are constrained by using the SHAKE algorithm[48].

In the following, the Valbond part is defined. A prerequisite for using Valbond is the skipping of angle definition which shall be managed by Valbond. Therefore, only angles of the imidazole ring atoms are defined but not the angle at the copper(I/II). The bond parameters between copper (I/II) and nitrogen was derived from the Charmm force field entry for the iron-nitrogen bond and adjusted to copper as previously for the tetra-ammonia copper complex[28], with an energy of 86.302 $\frac{kcal}{mol}$ and a force constant $k_{Cu-N\,bond}$ of $1.98\,{}^{kg}/_{s^2}$. The Valbond parameter for the N-Cu-N angle was chosen as the force constant $k_{VALBOND\,Cu-N} = 100\,{}^{kg}/_{s^2}$ and the weight factor $wt_{VALBOND\,Cu-N} = 1$, to weight the possible hybrid orbitals equally. Next the structure was minimized using the steepest descent method. A 10 ps incremental heating cycle from 0 to 300 K with heating steps of 15 K and time steps of 1 fs was simulated and the system was allowed to equilibrate for further 10 ps using a Verlet integrator with time step of 1fs. An 1 ns microcannonical molecular dynamic simulation followed, i.e. the number of atoms, the volume and the energy were kept constant as time goes on (NVE-ensemble). Each 50 fs, a frame of the systems coordinates was stored in the trajectory file for further analysis, given a total of 20.000 frames.

3.4. Charmm - DFTB3

Density functional tight binding[49, 15] third order approximation[14] (DFTB3) was performed for the same system to compare the outcome with Valbond due to the recent parametrization of copper for DFTB3[16, 28]. This will enable to refine the Valbond force field as well as allow testing the DFTB3 model. Again, a cubic water box with 30 Å edge length was used, whereas the water molecules were modeled classically using Charmm with TIP3P and kept rigid with SHAKE as before. Minimization, heating and equilibration was carried out as already specified for

Valbond, vide supra. Afterwards, a 250 ps canonical molecular dynamic simulation followed, i.e. the number of atoms, the volume and the temperature are kept constant as time goes on (NVT-ensemble). Also for the DFTB3 simulation frames of the system coordinates were stored continuously. Each 10 fs, a frame was saved, given a total of 25.000 frames.

3.5. Gaussian DFT - B3LYP

Density functional theory was used with the B3LYP 6-31 G (d,p) basis set[3, 4, 37] which is implemented in the Gaussian software package[13] for the parametrization efforts. Structures for the parametrization of Valbond-Trans were generated using the Gview module. The structures were then optimized to a minimum energy and the frequency of the vibrations were calculated. Informations about total energy and metal-ligand bond length of the copper(II) complexes were gathered for further analysis.

3.6. Valbond-Trans parametrization

3.6.1. Thermodynamic *trans* influence

The model capturing the thermodynamic *trans* influence presented in equation Equation 2.23 was parametrized using a training set of 169 structures consisting of 3 diastereoisomers each made out of 4 different ligands and 42 structures consisting of 2 diastereoisomers each with 2 different ligands (MX_2Y_2, cis/trans isomerism). The geometry of every isomer was optimized to a minimum and the molecular vibrations were calculated using a ground state DFT B3LYP model with the 6-31G (d,p) basis set of the software Gaussian. The library of copper(II) square planar complexes is made of combinations of 10 different ligands which include the following substances:

Anionic	Neutral
Br^-	PH_3
Cl^-	NH_3
${CH_3}^-$	H_2O
H^-	H_2S
F^-	2-methyl-pyridine

Table 3.1.: Model ligands used for a library of square planar Cu(II)-complexes.

The choice of model ligands was inspired by previous *trans* influence parametrizations of octahedral complexes[52], with exception of 2-methyl-pyridine which was included due to the diverse use of ligands of the pyridine family in organometallic chemistry and hydrogen sulfide because of the observed Cu-coordination of sulfur containing amino acids in plastocyanine.

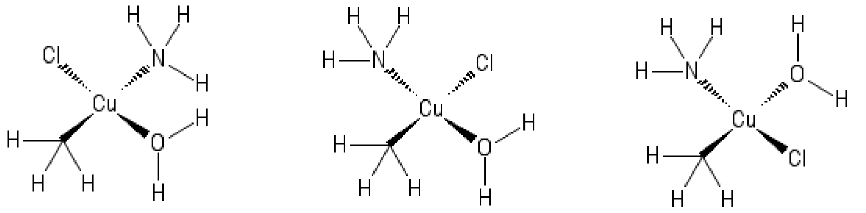

$\Delta E = 8.12 \, {}^{kcal}/_{mol}$ E_{min}- Isomer $\Delta E = 2.04 \, {}^{kcal}/_{mol}$

Figure 3.2.: Example of one isomer set build with chlorine, ammonia, aqua and alkyl ligands. The destabilizing effect of a ligand rearrangement is calculated with respect to the minimum energy, i.e. the most stable, isomer. The increase in potential energy is assign to the specific ligand composition and stored in a matrix covering all possible arrangements.

Table 3.2.: Example of the matrix entry for the copper(II)-complex presented in Figure 3.2. In each entry line, the two *trans* couples of the most stable isomer are listed with positive value 1, whereas the two *trans* couples of the destabilized complex are listed with negative values -1, also the associated increase in the potential energy is listed (isomerization energy difference ΔE). In case of the first line that means changing the ligands *trans* to each other from chloride-alkyl and ammonia-aqua to chloride-aqua and ammonia-alkyl is associated with an increased isomerization energy difference, hence a destabilization is observed which is caused by the *trans* influence.

P_{Cl-NH_3}	P_{Cl-H_2O}	P_{Cl-CH_3}	$P_{NH_3-H_2O}$	$P_{NH_3-CH_3}$	$P_{H_2O-CH_3}$	ΔE $[{}^{kcal}/_{mol}]$
0	-1	1	1	-1	0	8.12
-1	0	1	1	0	-1	2.04

A matrix was set up with respect to the most stable isomer (minimum energy isomer), as shown in Figure 3.2 and Table 3.2. The corresponding increase in isomerization energy due to different *trans* oriented ligands was assigned. A fit according to equation Equation 2.23 comparing the obtained DFT calculations with the model values was made by means of a least-squares procedure. Best agreement between both is achieved if all data points lie on a linear function $y = x$. The quality of the fit was measured by the root mean square deviation (RMSD)

$$RMSD = \sqrt{\frac{\sum_{t=1}^{n} \left(x_{DFT,t} - x_{model,t}\right)}{n}} \tag{3.2}$$

and mean absolute deviation (MAD)

$$MAD = \frac{1}{n}\sum_{t=1}^{n} |x_{model,\,t} - x_{DFT,\,t}| \tag{3.3}$$

3.6.2. Structural *trans* influence

To asses the *trans* influence on the ligand-metal distances, all bond lengths were extracted from the DFT calculations. Additionally, to find the unperturbed bond length, DFT calculations of Cu(II) complexes with ligands of one type exclusively were set up for each ligand type and the average bond length of the 4 ligand-metal bonds was used as r_0, the reference bond length value in the equation Equation 2.25 to model the *trans* influence. Including these, 2400 bond lengths obtained from B3LYP DFT calculations were used in a fit obtaining the sensitivity s_A and intensity i_B parameters for each ligand using a reduced gradient code[36] and a least-squares procedure. Best agreement between DFT derived bond length and model bond length is achieved if all data points lie on a linear function $y = x$.

3.7. Free energy calculations of the copper(I) oxidation in water

The parametrization of the copper(I) and copper(II) ion upon oxidation was carried out using the PERT [43] module of CHARMM. Two systems containing a copper ion within a cubic box with edge length of 30 Å and TIP3P water model as solvent were set up. The copper(I)-ion was mutated to copper(II) using a dual-topology-single-coordinate (DTSC) approach similar to reported QM/MM methods[39, 28] but using exclusively the CHARMM force field. The DTSC method uses a hybrid potential that is a combination of the potentials of the starting state, Cu(I) and the end state, Cu(II), using a coupling parameter λ

$$U(\lambda) = (1-\lambda)\,U_{Cu(II)} + \lambda U_{Cu(I)} = U_{Cu(II)} + \lambda\left(U_{Cu(I)} - U_{Cu(II)}\right) \tag{3.4}$$

Thermodynamic integration is used to calculate the change of the free energy, given by

$$\triangle F = \int_0^1 \frac{\partial F(\lambda)}{\partial \lambda} d\lambda = \int_0^1 \left\langle \frac{\partial F(\lambda)}{\partial \lambda} \right\rangle_\lambda d\lambda = \int_0^1 \left\langle \left(U_{Cu(I)} - U_{Cu(II)}\right) \right\rangle_\lambda d\lambda \tag{3.5}$$

where $\left(U_{Cu(I)} - U_{Cu(II)}\right) = \Delta E$ equals the energy gap. Here, 21 λ windows are used and each window was sampled for 21 ps. A correction of the obtained change in free energy was not considered.

4. Results and Discussion

4.1. Overview

First, in section 4.2 the findings of the parametrization for a Valbond-Trans force field applicable to copper(II) square planar complexes are presented and the graphically displayed results are discussed. Second, section 4.3 analyses the dynamics of the model compound copper(I/II)-imidazole$_4$ and parallel to this provides insights into the simulation quality by comparison of the purely classical Charmm-Valbond force field to the classical-quantum mechanical hybrid Charmm-DFTB3 calculation with respect to structural integrity, solvent interaction and the response to excitation. Lastly the investigations of the copper(I/II)-ion Lennard-Jones parameters are shown in section 4.4

4.2. Valbond-Trans parametrization

4.2.1. Parametrization of thermodynamic *trans* influence

The fitting procedure was carried out for all isomers with respect to the most stable isomer of each set. The more positive the $\triangle$E-value, the less stable is the isomer compared to the E$_{min}$-isomer of their set. Figure 4.1 shows the fit for all possible ligand arrangements, sorted according to the structures $\triangle$E. The Table 4.1 shows the quality measure of the fit based on calculated deviations from the DFT reference values. All possible ligand arrangements were considered, which include the following ligands: PH_3, Br^-, Cl^-, NH_3, H_2O, $CH_3{}^-$, H^-, 2-methyl-pyridine and F^-. Obviously, the fit lacks accuracy, given an RMSD of 3.110 $^{kcal}/_{mol}$ and an MAD of 2.264 $^{kcal}/_{mol}$. The derived parameters are presented in Appendix A at the end of the manuscript. Some DFT derived energy values which showed exceptional high differences are excluded from the plot, because they were considered as wrong calculated by DFT. The reason for that could be found in the use of the 6-31G(d,p) basis set for the whole complex instead of splitting the basis set, i.e. using the LANL2DZ effective core potential for the copper metal core and 6-31G(d,p) for the ligands.[19] Other than that, a big portion of calculations carried out with PH_3 and/or Br^- or Cl^- and H_2S showed dissociative behavior or adopted a tetrahedral conformation instead of a square planar one. The cause of that could be the high electron density of the anionic ligands bromide and chloride and their larger spatial expansion. This pushes the loosely coordinated hydrogen sulfide away from the copper core, which is due to anionic ligands already decreased in cationic property or may even adopt a negative partial charge. However, a noticeable number of these chemically unfavored structures were successfully calculated and give rise to a number of points with isomerization energy differences at about 0 $^{kcal}/_{mol}$ in the DFT calculation, playing a significant role for the fitting procedure. Therefore, several subsets were created, started by covering only a narrow chemical space to a broader one.

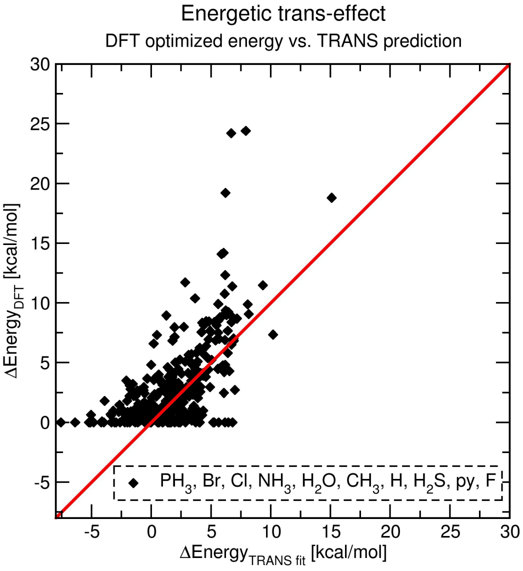

Figure 4.1.: Full set fit containing all created structures.

Subset 1 Subset 1, Figure 4.2, consist of isomers build with ligands Cl^-, NH_3, H_2O, $CH_3{}^-$, H^- exclusively. This subset resulted in parameters for Equation 2.23 which reproduces the DFT calculated energies well, $RMSD_{subset\,1}$=0.981 $^{kcal}/_{mol}$ and $MAD_{subset\,1}$=0.718 $^{kcal}/_{mol}$.

Subset 2 Subset 2, middle left in figure Figure 4.3, consist of isomers build with ligands Cl^-, NH_3, H_2O, $CH_3{}^-$, $H^-$and F^-. This enhance the robustness of the model fit with passable costs for the accuracy, $RMSD_{subset\,2}$=1.611 $^{kcal}/_{mol}$ and $MAD_{subset\,2}$=1.117 $^{kcal}/_{mol}$.

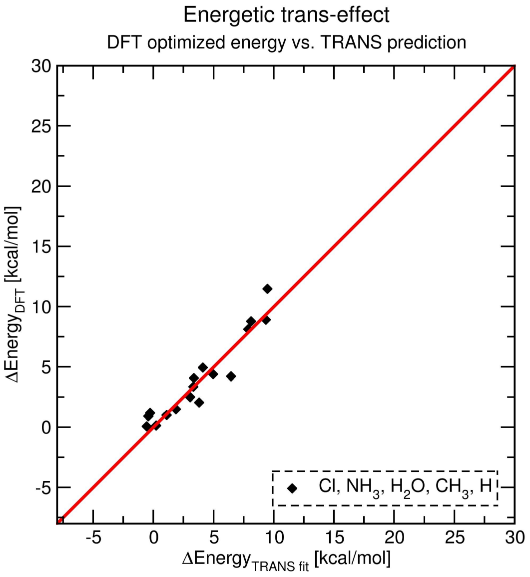

Figure 4.2.: Subset 1 with ligands from a reduced basis. This results in an both 68% improved RMSD and MAD compared to the full set.

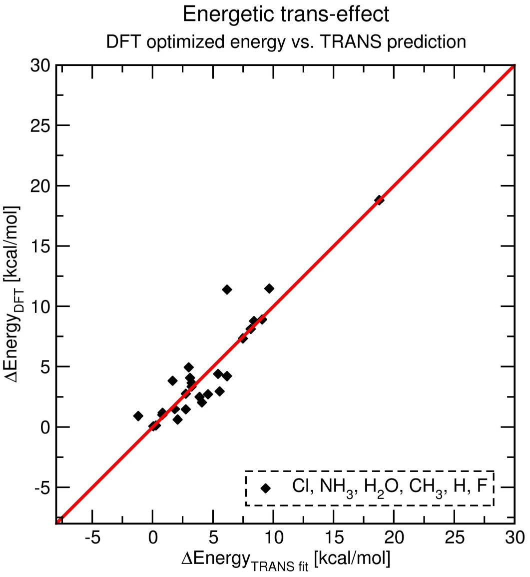

Figure 4.3.: Subset 2 covers the ligands from subset 1 plus fluoride. This results in an 48% improved RMSD and a 50% MAD compared to the full set.

Subset 3 Subset 3, middle right in figure Figure 4.4, contains isomers build with ligands Cl^-, NH_3, H_2O, $CH_3{}^-$, H^-, F^- and 2-methyl-pyridine. The inclusion of 2-methyl-pyridine increase the number of data points which spread more on both sides of the linear function drawn in red, increasing $\mathrm{RMSD}_{subset\,3}$=2.488 $^{kcal}/_{mol}$ and $\mathrm{MAD}_{subset\,3}$=1.837 $^{kcal}/_{mol}$.

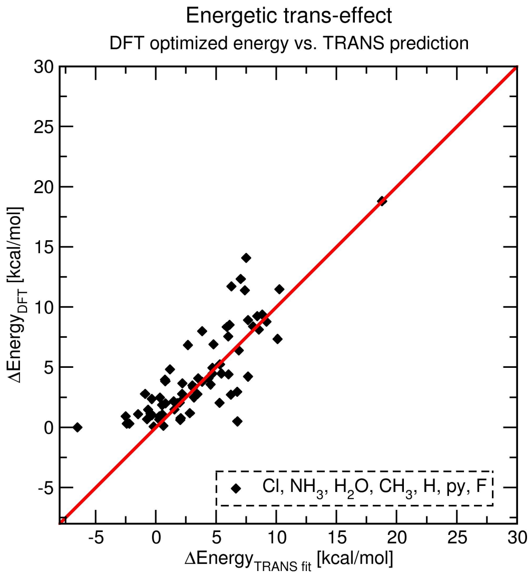

Figure 4.4.: Subset 3 contains in addition to subset 1 fluoride and 2-methyl-pyridine. This results in an 20% improved RMSD and a 19% MAD compared to the full set.

Subset 4 Subset 4, lower left in Figure 4.5, contains the minimum subset 1 and hydrogen sulfide in addition to be able to investigate copper coordination of sulfur ligands. As mentioned in the discussion of the full set, inclusion of H_2S is associated to the creation of non planar complex geometries if chloride, bromide and/or phosphine were present. For the latter two, even dissociative behavior was observed. Despite this, interaction with chloride in absence of bromide or phosphine seems not that strong and reasonable structures are found by DFT optimization. Therefore, hydrogen sulfide was included in this fit, rising the $\mathrm{RMSD}_{subset\,4}$=1.739 $^{kcal}/_{mol}$ and $\mathrm{MAD}_{subset\,4}$=1.408 $^{kcal}/_{mol}$ from the lower values of subset 1, $\mathrm{RMSD}_{subset\,1}$=0.981 $^{kcal}/_{mol}$ and $\mathrm{MAD}_{subset\,1}$=0.718 $^{kcal}/_{mol}$. Still, the gain in coverage of chemical space is outperform the loss in accuracy.

Subset 5 Motivated by the findings of subset 1 - 4, subset 5 in Figure 4.6, combines all previously ligand types to obtain a model which lacks only phosphine and bromide compared to the initial full fit. The parameters derived from subset 5 fit are considered for further improvement of the *trans* parameters. The $\mathrm{RMSD}_{subset\,1}$=2.418 $^{kcal}/_{mol}$ and $\mathrm{MAD}_{subset\,1}$=1.839 $^{kcal}/_{mol}$.

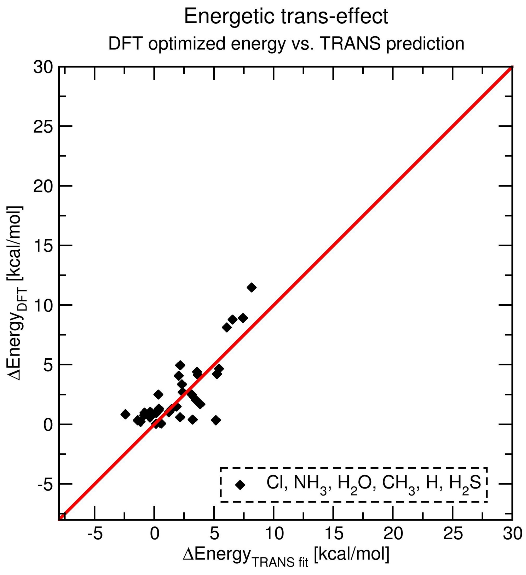

Figure 4.5.: Subset 4 pictures the dramatic effects if hydrogen sulfide is included. This results in an 44% improved RMSD and a 37% MAD compared to the full set. Comparison with the subset 1 illustrate the negative impact of the H_2S inclusion into the fit: the RMSD is 77% m the MAD 96% higher.

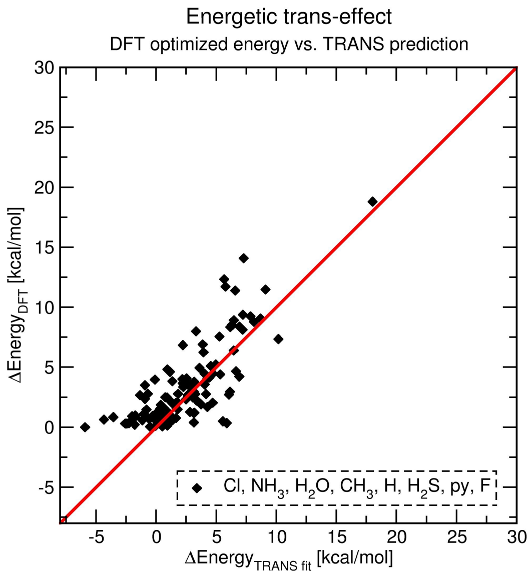

Figure 4.6.: Subset 5 resulted in passable energetic trans parameters and can thus considered for further investigation. The exclusion of phosphine and bromine leads to an 28% improved RMSD and a 23% MAD compared to the full set.

Table 4.1.: Fit quality, root mean square deviation (RMSD) and mean absolute deviation (MAD). The full fit includes isomers of copper(II) complexes with the following ligands: PH_3, Br^-, Cl^-, NH_3, H_2O, $CH_3{}^-$, H^-, 2-methyl-pyridine and F^-. Subset 1 consist of isomers build with ligands Cl^-, NH_3, H_2O, $CH_3{}^-$, H^- exclusively. Subset 2 contains additionally to this structures build with F^-. Subset 3 contains isomers build with ligands Cl^-, NH_3, H_2O, $CH_3{}^-$, H^-, F^- and 2-methyl-pyridine. Subset 4 contains Cl^-, NH_3, H_2O, $CH_3{}^-$, H^- and H_2S, inclusion of hydrogen sulfide decreases the fit accuracy. Subset 5 contains all mentioned ligands, i.e. like the full fit but PH_3 and Br were excluded as these ligands lead to dissociation of hydrogen sulfide.

	RMSD $[{}^{kcal}/_{mol}]$	MAD$[{}^{kcal}/_{mol}]$
Full	3.110	2.264
Subset 1	0.981	0.718
Subset 2	1.611	1.117
Subset 3	2.488	1.837
Subset 4	1.739	1.408
Subset 5	2.418	1.839

4.2.2. Parametrization of structural *trans* influence

The same structures used for the parametrization of the thermodynamic *trans* influence were used to observe the structural *trans* influence which is modeled by Equation 2.25. Table 4.2 overviews the RMSD and MAD of each subset, whereas in Appendix A the fitting parameters of each ligand, normalized with respect to chloride, and deviation values are given. In Figure 4.7 the same arrangement as before is shown, upper left corner the full set. Again, the quality of the fit is insufficient, especially if one considers the atom distances observed by DFT at nearly 4 Å, which can be considered as loosely coordinated. To analyze the findings, the same subset comparison as before can be done.

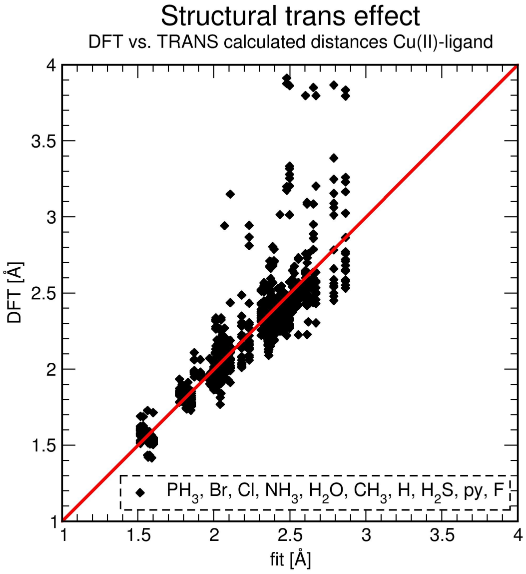

Figure 4.7.: Structural *trans* influence, full set with all successfully calculated structures. Fit RMSD=0.140 Å , MAD=0.084Å.

Subset 1 In subset 1, shown in Figure 4.8, the Cu-H distance is well reproduced at around 1.6 Å as well as the Cu-N distances at around 1.9-2.0 Å. The distance Cu-O is modeled to be extended if it stands *trans* to $C^{CH_3^-}$, leading to a modeled distance of Cu-$O^{H_2O\,trans\,CH_3^-}$=2.25 Å which is an increase of 0.31 Å compared to the unperturbed distance but this conclusion is biased from one DFT derived distance outlier of 2.86 Å. Nevertheless, the 4 remaining DFT distances also indicate a lengthening by 0.26 Å. Consequently, the distance Cu-$C^{CH_3^-\,trans\,H_2O}$ is shortened by -0.17 Å (DFT) respectively by -0.04 Å (model). The behavior is observed if chlorine stands *trans* to aqua, the Cu-$O^{H_2O\,trans\,Cl^-}$ is increased by 0.17/0.23 Å (DFT/model). The corresponding bond shortening of Cu-$Cl^{Cl^-\,trans\,H_2O}$ is not recognized by the fit, -0.13/+0.01 Å (DFT/model). Furthermore lengthening of Cu-$O^{H_2O\,trans\,H^-}$ by 0.31/0.29 Å (DFT/model) is observed. Oxygen^{H_2O} exhibit a clear *trans* influence, its bond to copper is weakened by carbon$^{CH_3^-}$, chloride and hydride. Nitrogen^{NH_3} does not show a prominent *trans* influence and stays relative stable, only a small perturbation of 0.04 Å is observed if *trans* to chloride. All other *trans* combinations do not influence the copper-nitrogen distance, also nitrogen do not induce a distance change in other ligands. Chloride showed a clear *trans* influence with aqua, as shown before but the model fit do not capture this influence (points at 2.35 Å of fit-axis below red line). The fitted chloride distances deviate from the DFT calculated ones. e.g. in two of seven structures where C$^{CH_3^-}$ stands trans to Cl$^-$, the DFT values getting as high as 2.70 Å while getting also down as low as 2.19 Å. Such deviations makes a prediction with the used Trans model a difficult task.

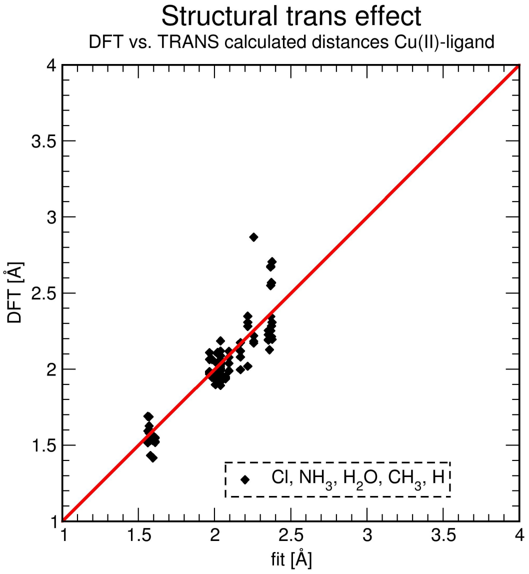

Figure 4.8.: Subset 1, only structures with chloride, ammonina, aqua, alkyl and hydride ligands are included. Fit RMSD=0.113 Å , MAD=0.083Å.

Subset 2 The inclusion of fluoride, see Figure 4.9, adds a cluster of data points for the fitting a around 1.87 Å and is well reproduced by the TRANS model. Comparison of the data showed that the Cu-F$^{-F^{-}\,trans\,H_2O}$ distance is shortened by -0.08/-0.03 Å (DFT/model) and the Cu-F$^{-F^{-}\,trans\,NH_3}$ distance by -0.09/-0.05 Å (DFT/model). The effect on the Cu-F^{-} bond by hydride is overestimated by the model, $\triangle$Cu-F$^{-F^{-}\,trans\,H}$=-0.03/-0.07 Å. Fluoride exhibit a *trans* influence with aqua, ammonia and hydride ligands.

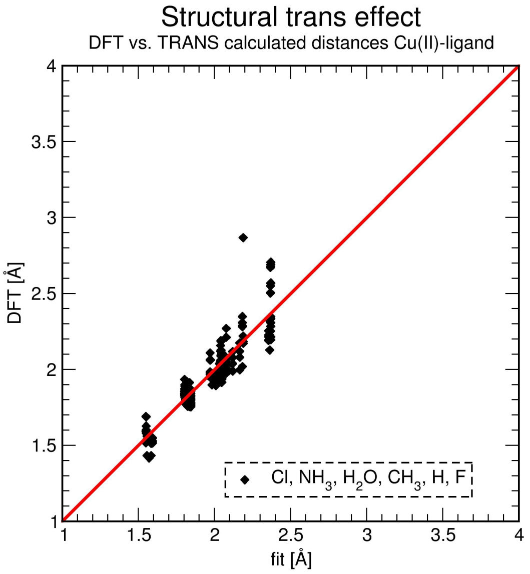

Figure 4.9.: Subset 2, structure library of subset 1 was extended with fluoride, which showed a structural *trans* interaction with hydride, ammonia and aqua ligands. The overall fit quality is improved compared with the subset 1 as well is more chemical space covered. Fit RMSD=0.094 Å , MAD=0.066Å

Subset 3 Subset 3, Figure 4.10, includes in addition to subset 2 the 2-methyl-pyridine ligand with a unperturbed bond length of around 1.98 Å. Overall, this ligand is less sensitive to the *trans* influence than others but if it strands *trans* to alkyl, the bond length is even more perturbed than observed for chloride and fluoride. DFT calculation revealed a bond lengthening mediated by alkyl of +0.08 Å compared with a TRANS model bond lengthening by +0.05 Å.

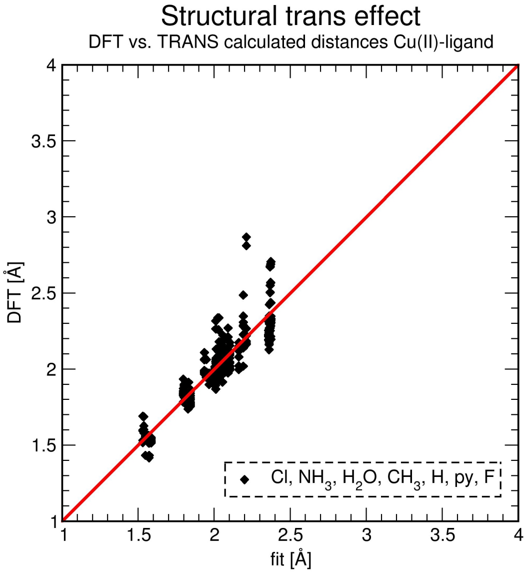

Figure 4.10.: Subset 3, the structure library of subset 2 was extended with 2-methyl-pyridine, which showed a more distinct structural *trans* interaction with alkyl as with chloride and fluoride ligands. The overall fit quality is improved compared with the subset 1&2 due to the good agreement of the resulting complexes. Fit RMSD=0.090 Å , MAD=0.064Å

Subset 4 Subset 4, Figure 4.11, includes in addition to subset 1 hydrogen sulfide (H_2S). As expected, the influence of the hydrogen sulfide ligand is most prominent: The model prediction of the distance of Cu-$H_2S^{H_2S\,trans\,CH_3^-}$ at 2.88 Å is insufficient while the DFT calculation resulted in distances of 2.5-3.8 Å, at which the both cases of ~3.8 Å can be considered as not bonded, if one assumes $r_{S_{VdW}}$=1.8 Å and $r_{Cu^{II\,2+}_{VdW}}$=0.7 Å. Overall, the interaction of copper with hydrogen sulfide can be considered as more or less strongly coordinated. Also, the fit distance Cu-$H_2S^{H_2S\,trans\,H^-}$ at 2.83 Å captures only a small part of the DFT calculated distances, which rises up to 3.9 Å. Nevertheless, the plastocyanin relevant Cu-$H_2S^{H_2S\,trans\,N^{NH_3}}$ and Cu-$H_2S^{H_2S\,trans\,N^{py}}$ distance of the fit is with 2.48/2.60 Å in suitable agreement with the DFT obtained values of 2.51/2.61 Å.

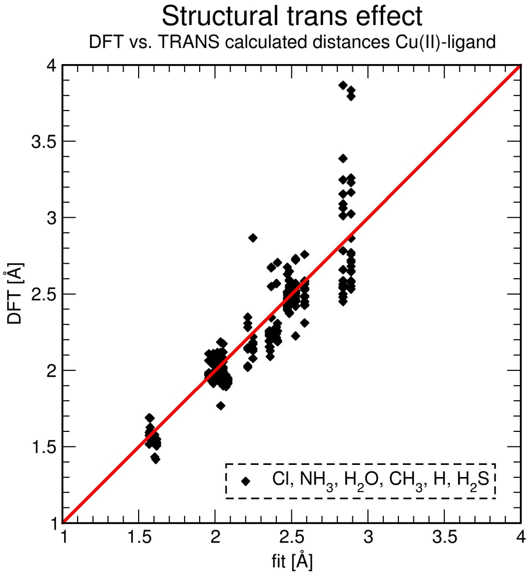

Figure 4.11.: To obtain subset 4, subset 1 was extended with hydrogen sulfide to examine the effects. H_2S show strong interaction with alkyl and hydride. DFT derived data suggest a loosely coordination of hydrogen sulfide. The overall fit quality is worsen compared with subset 1 due to scattered values. Fit RMSD=0.162 Å , MAD=0.107Å

Subset 5 The foregoing mentioned subsets combined results in subset 5, Figure 4.12, whereas the hydrogen sulfide related data points lower the quality of the fit, see Table 4.2. It should be noted that especially the copper(II)-hydrogen sulphide interaction can not be described as bonded but rather as coordinated. A bond like distance is observed if a nitrogen ligand is *trans* to the hydrogen sulfide. Due to the broader coverage of chemical space and the possible application of TRANS parameters of these fits for proteins with copper as prosthetic group, hydrogen sulfide was included to subset 5 in addition to the well performing fluoride and 2-methylpyridine.

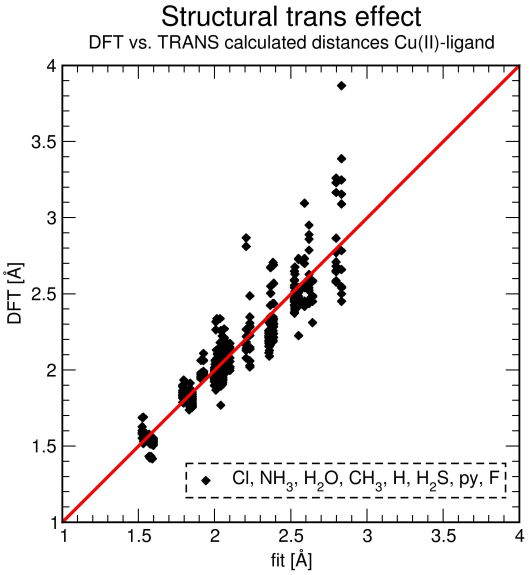

Figure 4.12.: Subset 5 contains only structures with chloride, ammonium, aqua, alkyl, hydride, 2-methyl-pyridine, fluoride and hydrogen sulfide ligands. Bromide and phosphine were excluded to obtain for the remaining ligands the best Trans parameters of the given data. The fit quality is improved compared to the initial one, RMSD=0.112 vs 0.140 Å and MAD=0.077 vs. 0.084 Å (subset 5 vs. full set), due to a big number of well performing complexes with 2-methyl-pyridine ligands, while covering a broad chemical space.

Table 4.2.: Fit quality, root mean square deviation (RMSD) and mean absolute deviation (MAD). The full fit includes isomers of copper(II) complexes with the following ligands: PH_3, Br^-, Cl^-, NH_3, H_2O, $CH_3{}^-$, H^-, 2-methyl-pyridine and F^-. Subset 1 consist of isomers build with ligands Cl^-, NH_3, H_2O, $CH_3{}^-$, H^- exclusively. Subset 2 contains additionally to this isomers build with F^-. Subset 3 contains isomers build with ligands Cl^-, NH_3, H_2O, $CH_3{}^-$, H^-, F^- and 2-methyl-pyridine ligands. Subset 4 contains Cl^-, NH_3, H_2O, $CH_3{}^-$, H^- and H_2S, inclusion of hydrogen sulfide decreases the fit accuracy. Subset 5 contains all mentioned ligands, i.e. from the full fit, PH_3 and Br^- were excluded as these ligands lead to miscalculated complexes.

	RMSD [Å]	MAD [Å]
Full	0.140	0.084
Subset 1	0.113	0.083
Subset 2	0.094	0.066
Subset 3	0.090	0.064
Subset 4	0.162	0.107
Subset 5	0.112	0.077

4.3. Copper(I/II)-imidazole$_4$ dynamics using Valbond vs. DFTB3/MM

The dynamics of a Copper(I/II)-imidazole$_4$ system was investigated using VALBOND and DFTB3, the latter a new developed quantum mechanical method. Structural properties and the interaction with the solvent water was of interest. Also the excitation of the copper(I) complex to a copper(II) complex was investigated.

First, the bond distances of copper(II)-imidazole$_4$ were compared by reported distances obtained from X-ray crystal structures and X-ray absorption spectra (XAS), see Table 4.3. Lin *et al.*[41] reported two slightly different bond length but the study was conducted on a octahedral geometry, focusing on the Jahn-Teller distortion of Cu(II) complexes, where the axial bonds are 0.2 to 0.6 Å longer than the four bonds in the equatorial coordination plane. Furthermore, between neighboring imidazole rings a coordination of hydrogen towards the π system of the next ring is observed, C-H$\cdots\pi$. The from X-ray crystal structures reported bond distance of the pair Cu(II)-N$_{imidazole_A}$=1.996 Å varies slightly compared with the neighboring pair Cu(II)-N$_{imidazole_B}$=2.036 Å. Another report by Frank *et. al*[12] conducted with XAS postulates a Cu-N$_{imidazole}$ distance of 2.02Å for all four ligands. In this work, the DFT B3LYP 6-31 G (d,p) calculated distance was 1.984 Å and 1.986 Å (pairwise), the average over a 1 ns VALBOND simulation resulted in 1.983 Å (all four ligands) and the average over a 250 ps SCC-DFTB3 simulation resulted in 1.968 Å and 2.049 Å (pairwise). The pairwise splitting of the bond length is successfully captured by the DFTB3 method and the observed bond length differs only by 1.4% and 0.6% from the X-ray crystal model. VALBOND delivers a value deviating 1.6% from the averaged pairwise X-ray value. Thus, both methods are regarded as suitable to catch the bio-inorganic bond of copper with imidazole ligands. In Figure 4.13, the flexibility of the ligands is shown as dihedral angle. The DFTB3 simulation deliver more flexible structures compared to the VALBOND simulation at room temperature. Testing the force field accuracy, atom-atom distances of minimized structures of both VALBOND and DFTB3 were compared to X-ray derived atom distances. The results showed slightly better agreement between the VALBOND minimized structure and the X-ray crystal, see Figure 4.14.

Table 4.3.: Bond length comparison Cu(II)-Imidazole$_4$. Average bond length of 1 ns VALBOND simulation of Cu(II)-Imidazole$_4$ solvated in water compared with the reported X-ray bond length by Lin *et al.[41]* and XAS by Frank *et al.*[12] and with bond length obtained by DFT calculation with the B3LYP basis set and with the average of 250 ps SCC-DFTB3 calculation. The reported X-ray difference is best reproduced by SCC-DFTB3 calculations. N$_1$ neighboring N$_2$, values for N$_{1/2}$ are average of both bond length trans to each other.

	Cu-N$_1$	Cu-N$_2$
reported X-ray crystal[41]	1.996	2.036
reported XAS[12]	2.02	2.02
1 ns VALBOND - Dynamics	1.983	1.983
250 ps SCC-DFTB3 - Dynamics	1.968	2.049
DFT B3LYP - Optimized structure	1.984	1.986

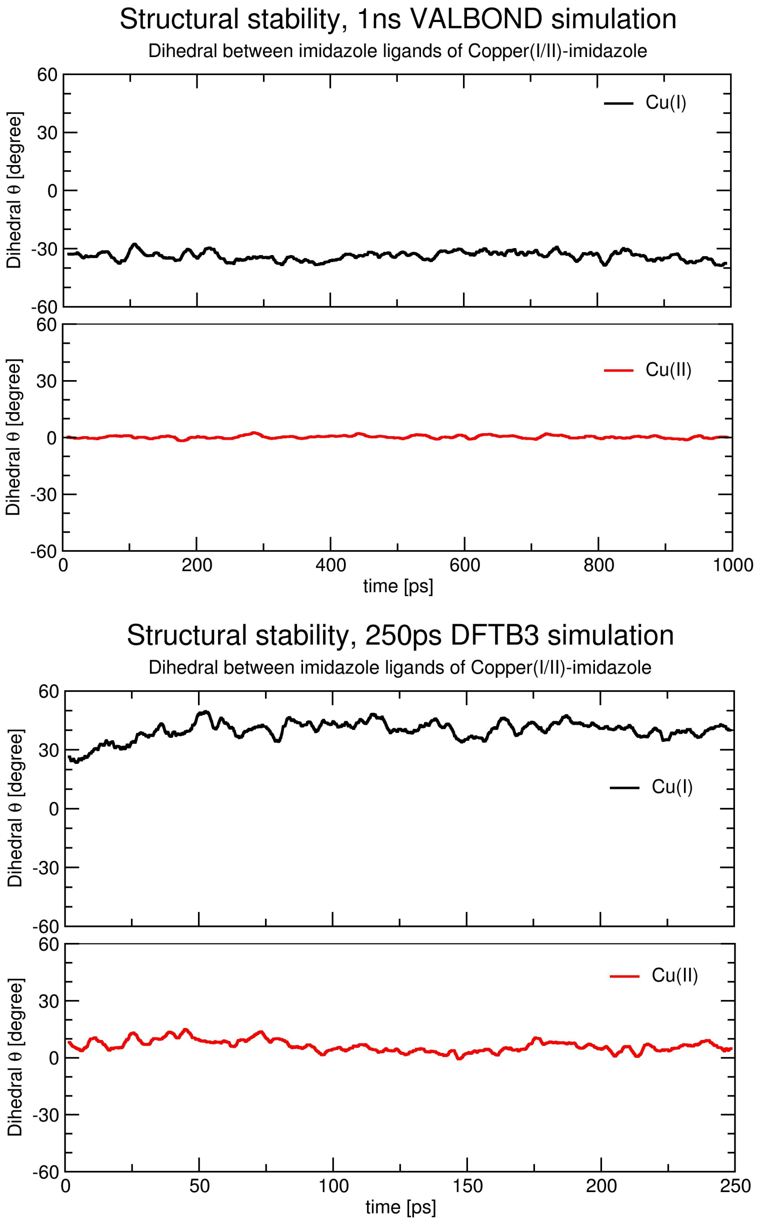

Figure 4.13.: Thermal caused structural fluctuations of Cu(I/II)-imidazole represented by the dihedral between the imidazole ligands connected by the copper core ($\phi\,(Cu - N - N - N)$), top from 1ns VALBOND, bottom from 250 ps DFTB3 simulations. The tetrahedral copper(I)-imidazole fluctuates a bit more than the square planar copper(II)-imidazole in both cases but in the DFTB3 simulation the tetrahedral geometry is not as rigid as shown by the VALBOND simulation. Moving averages of 15 ps for VALBOND and of 3 ps for DFTB3.

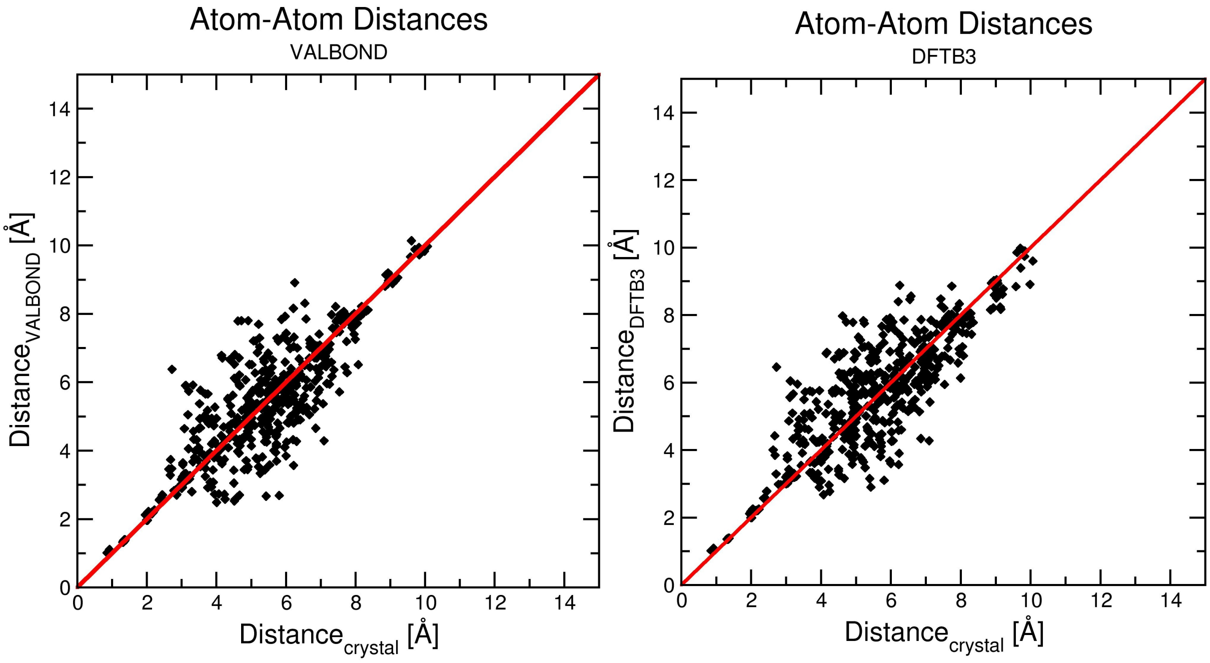

Figure 4.14.: Atom-atom distances of minimized structures, calculated using VALBOND (left) or DFTB3 (right), against X-ray crystal atom-atom distances. The less extended points cloud and better matching points for longer atom-atom distances for the VALBOND minimized structure with the X-ray reported distances indicates the good performance of VALBOND.

Second, the performance in solvation was studied. Using VMD[26], the number of water molecules around a certain spherical distance from the copper core was analyzed and summarized in Table 4.4. From XAS data, one would expect to see 3 different solvation schemes for copper(II)-imidazole$_4$: Two water molecules strongly coordinated at the axial positions, two additional within 4 Å and 6 water molecules finalizing the solvation shell within 4.4 Å. Both VALBOND and DFTB3 misses the 10 water molecules within 4.5 Å but catches these within 5.5 Å. The probability of water distribution for the VALBOND simulation is shown in Figure 4.15 for the Cu(I) and Cu(II) complex. In a comparison of partial charge schemata for VALBOND was NBO found to better reconstruct the solvation shell than Mulliken partial charges, see Figure 4.16 presenting the radial distribution function of water around the copper core. The peaks in $g_O(r)$ indicates a water solvation shell and $N_O(r)$ displays the number of water molecules within that shell. Figure 4.17 compares $g_O(r)$ and $N_O(r)$ of VALBOND with NBO partial charges with DFTB3. The solvation is less prominent in the DFTB3 calculations as well as the number of water molecules are. This could be related to geometrical effects as the classical calculations showed more rigid complexes and thus allow to stay water molecules closer to the copper, see Figure 4.13. Whereas in VALBOND the copper(II) complex is easier coordinated by water, in DFTB3 both complexes are equally coordinated. In Figure 4.18, lower left figure, and in Figure 4.19 one can see that the tetrahedral geometry of copper(I)-imidazole$_4$ is distorted. The same holds true for the square planar copper(II)-imidazole$_4$, see Figure 4.20. Fluctuations of the complex caused by thermal excitation allows a less good coordination of water compared to the VALBOND findings.

Table 4.4.: Solvation shell comparison of Copper(I/II)-Imidazole complexes, derived from 1 ns VALBOND calculations and 250ps DFTB3 calculations. The values reflect the most frequently observed number of water molecules within a given distance around the copper atom for the total simulation time obtained from histograms. X-ray absorption spectroscopy of solvated Cu(II)-Imidazole modeled as square pyramidal with one axial bound water and another axial non bonded interaction with water is reported to have distances of 2.12 and 2.87 Å. Furthermore, 8 water molecules are reported to solvate the complex in two shells: 2 H_2O within 3.83 Å and 6 more H_2O within 4.40 Å. VALBOND captures the two water molecules close to the copper core, but misses the reported solvation shell.

no. of H_2O molecules within		3.5 Å	4.5 Å	5.5 Å
reported [12]	Cu(II)	2	10	-
Mulliken	Cu(I)	0	2	10
charge	Cu(II)	2	3	12
NBO	Cu(I)	0	4	12
charge	Cu(II)	2	5	14
DFTB3	Cu(I)	1	3	10
	Cu(II)	1	3	10

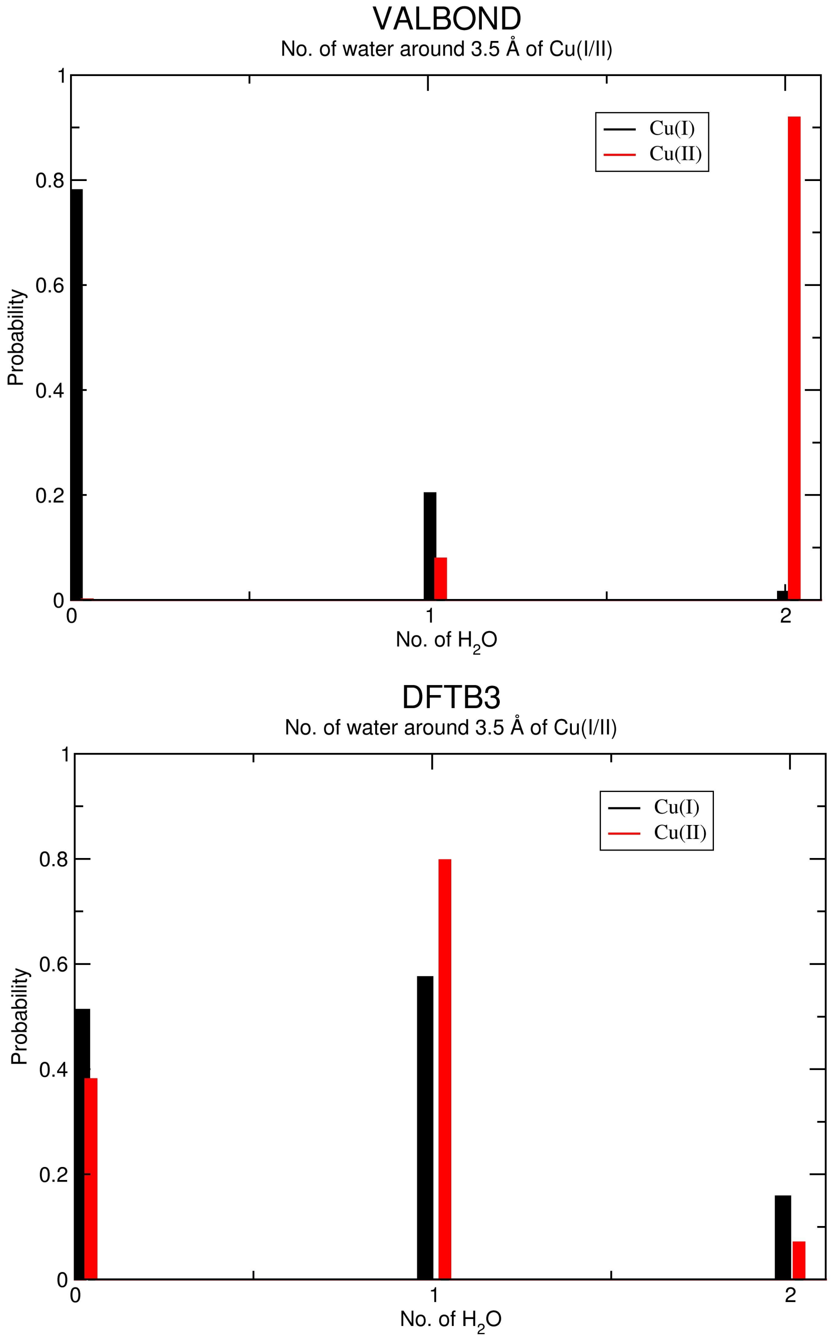

Figure 4.15.: Distribution of water molecules around 3.5 Å of Copper(I/II) obtained from 1ns equilibrium simulations with Valbond (top) and 250 ps equilibrium simulation with DFTB3 (bottom).

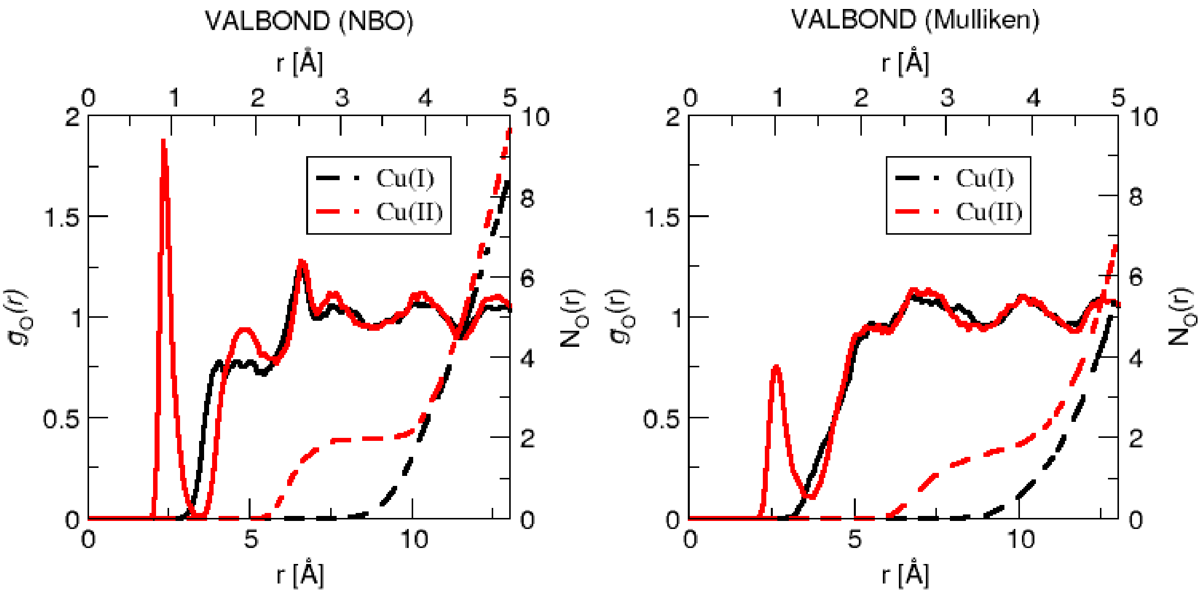

Figure 4.16.: Radial distribution function, Oxygen^{water} around the copper core of Cu(I/II)-imidazole$_4$, $g_O(r)$ within 15 Å, bottom and left axis. $\int g_O(r) = N_O(r)$, the number of water molecules within 5 Å, upper and right axis. The left graph is obtained from 1ns Valbond simulations using NBO partial charges from initial DFT optimization whereas the right graph is obtained from 1ns Valbond simulations using Mulliken partial charges. Copper(II)-imidazole$_4$ is expected to coordinate two water molecules at its axial positions, as reported by [12], see also Table 4.4. Therefore, NBO charges are considered to reproduce the solvation better.

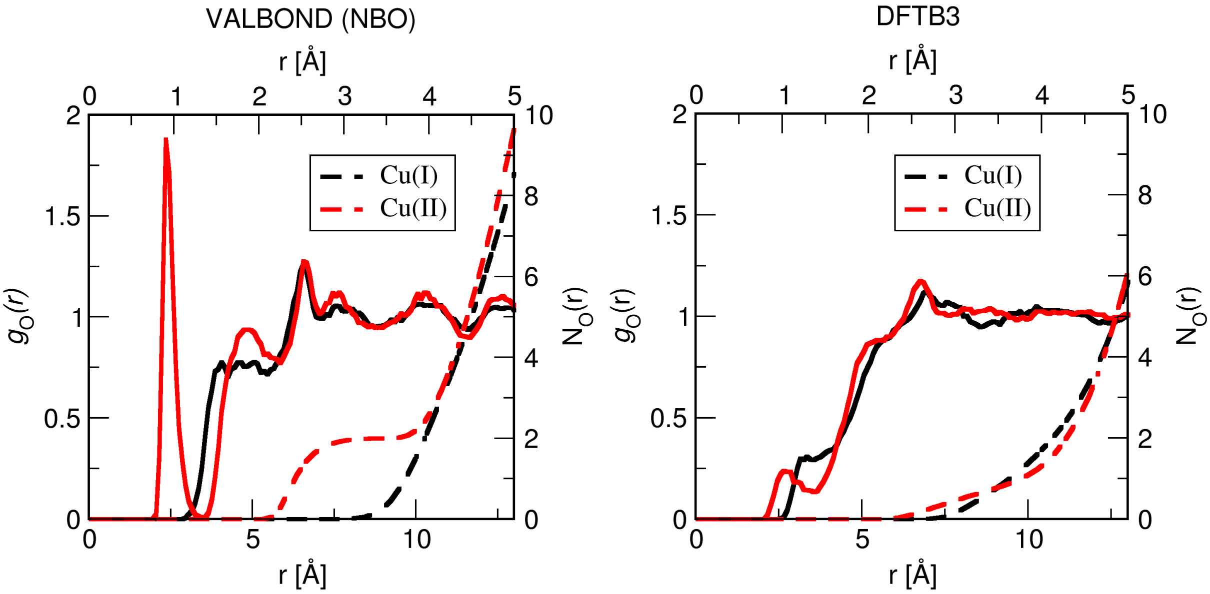

Figure 4.17.: Radial distribution function, Oxygen^{water} around the copper core of Cu(I/II)-imidazole$_4$ calculated with DFTB3. Compared to the VALBOND simulation, the Cu(II)-imidazole complex is geometrically more isolated, therefore the observed two water molecule coordination is not reproduced in DFTB3.

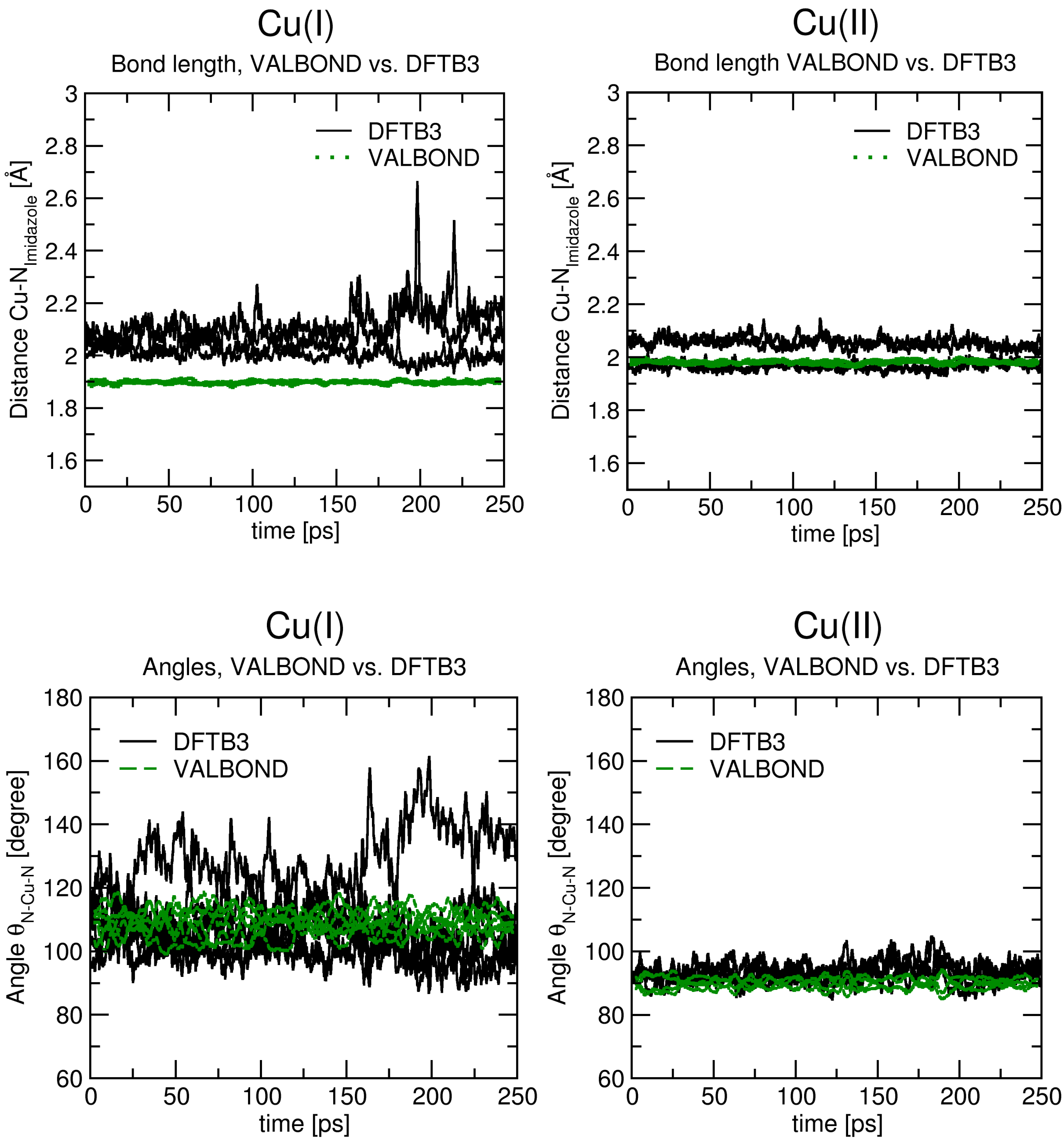

Figure 4.18.: Structural fluctuations of Cu(I/II)-imidazole$_4$ represented by the bond distance between imidazole ligand and copper (top) and represented by the N-Cu-N angle. Noticeable, upon thermal excitation the DFTB3 simulation reveals a more fluctuative copper(I) complex, both bond length and bond angles are deviating from their initial values and are changing over time more than compared with Valbond derived values. Moving averages of 1 ps for DFT, 5ps for Valbond, 250 ps simulation time presented in all cases.

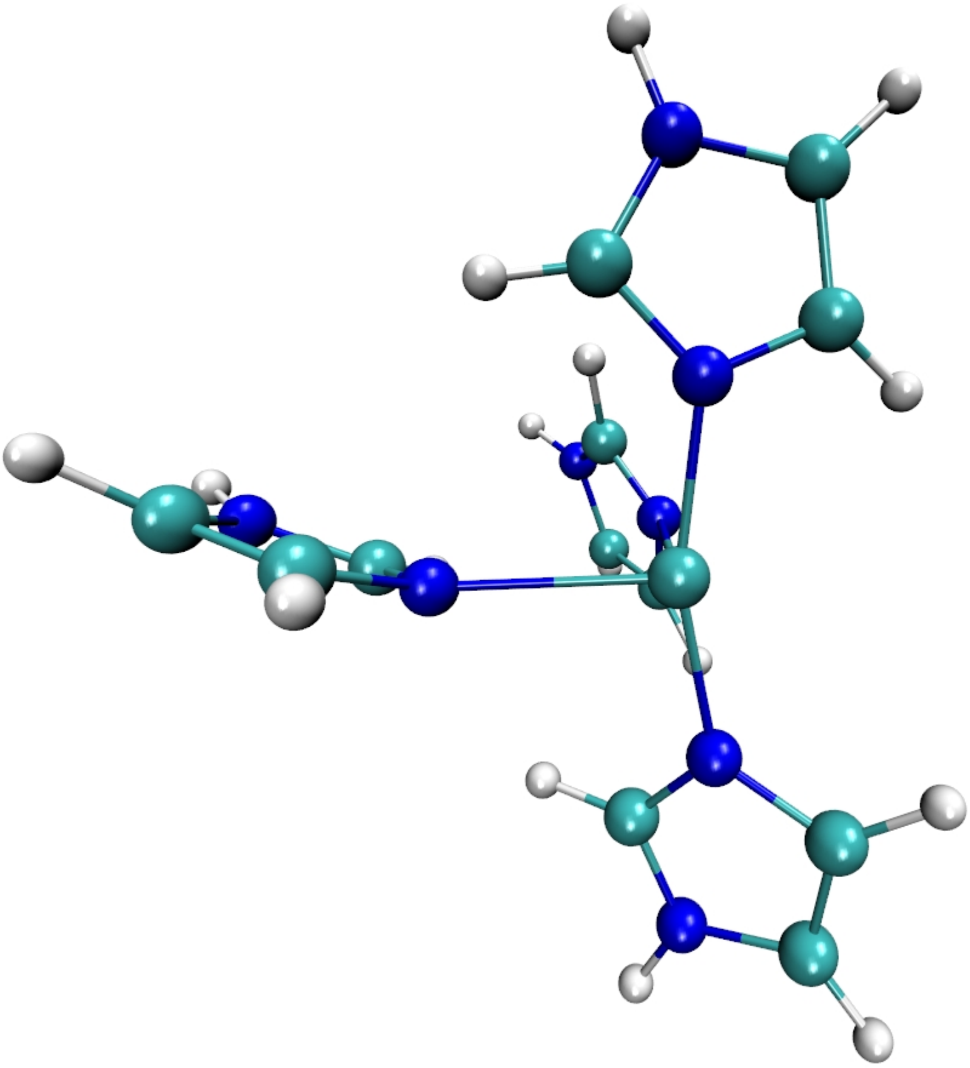

Figure 4.19.: Snapshot of copper(I)-imidazole after 200 ps DFTB3 simulation at room temperature. The tetrahedral geometry is thermally distorted and thus a different water solvation is observed.

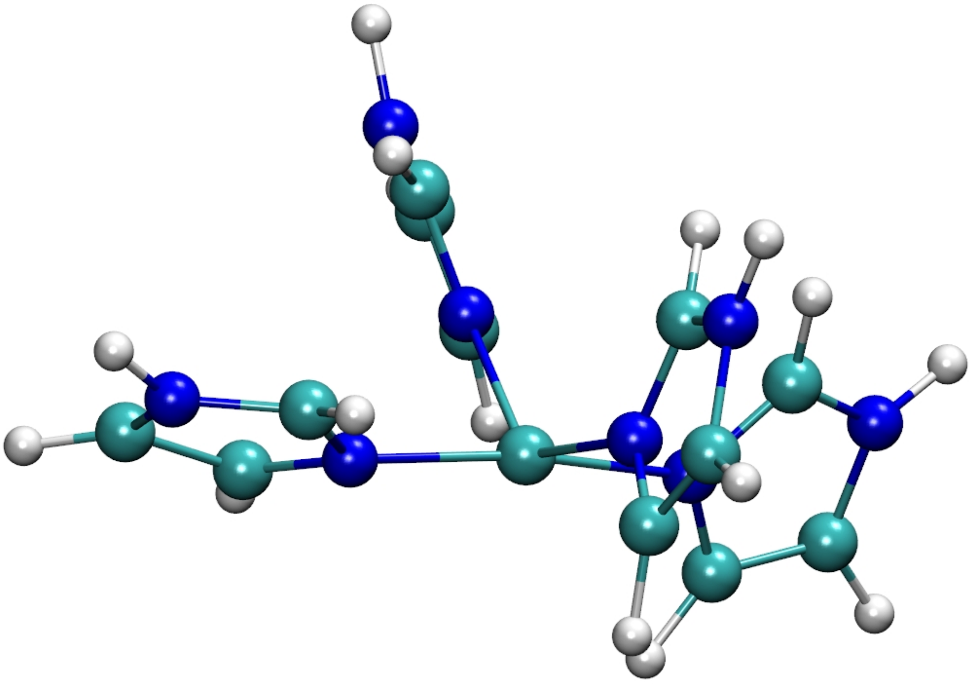

Figure 4.20.: Snapshot of copper(II)-imidazole after 200 ps DFTB3 simulation. The square planar geometry is thermally distorted and thus do not allow the experimental reported two water molecule coordination.

Motivated by the findings of Jin *et. al*[28], a non-equilibrium simulation was carried out. Recent experiments[46, 53] suggest that the structural changes and responses of the surrounding solvent upon changing the oxidation state occur within picoseconds. For the simulation, in both Valbond and DFTB3 the oxidation state of copper was changed from (I) to (II) in a copper(I) equilibrated environment. In Figure 4.21 the geometrical shift from copper(I) to copper(II) complex is depicted by the change of the N-Cu-N angle. The complete structural change is accomplished using Valbond within a picosecond, DFTB3 predicts a smooth transition with 5 picoseconds. The solvent response for Valbond is shown in Figure 4.22 and Figure 4.23. The rearrangement of the solvation shell happens directly after the structural change is complete (1 ps) and vast changes in the shell occur within 500 fs. Therefore, 1.5 ps after the excitation, the shell is in the midst of a transition which is completed 4 ps after excitation and equals the Cu(II)-imidazole$_4$ equilibrium. For the same solvent response but oxidizing the smaller Cu(I)-$(NH_3)_4$, a complete shell rearrangement with three picoseconds is reported[28].

In terms of computation time, the Valbond method is rather fast compared to DFTB3, a 250 ps calculation last for 1h using 16 central processing units (CPU) both for Cu(I) and Cu(II). DFTB3 calculations are in terms of computation more expensive. For copper (I), which has only paired electrons, a 250 ps simulation lasted for 19h using 16 CPUs, while for copper(II), which unpaired electron makes the calculation more complex, 33h are necessary.

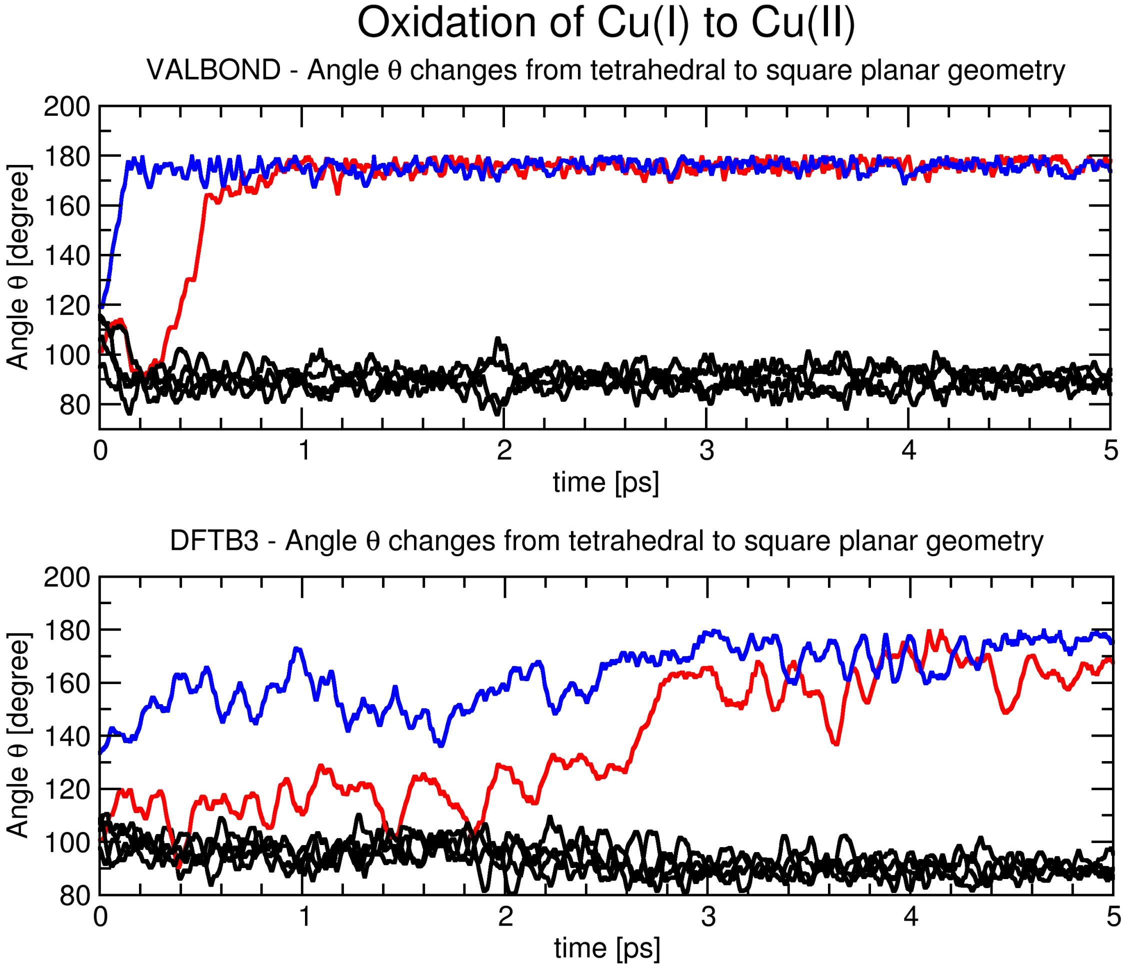

Figure 4.21.: Excitation of Cu(I)-imidazole$_4$: Oxidation of Cu(I) to Cu(II) results in a dramatic change in the geometry, i.e. from tetrahedral to square planar. Therefore, 2 angles have to stretch towards 180 degree leaving four angles at about 90 degree. On the top Valbond, bottom DFTB3. The time-scale of the geometrical change differs substantially, whereas Valbond predict around 1 pico second for the full shift, DFTB suggest a more flexible shift within 5 ps.

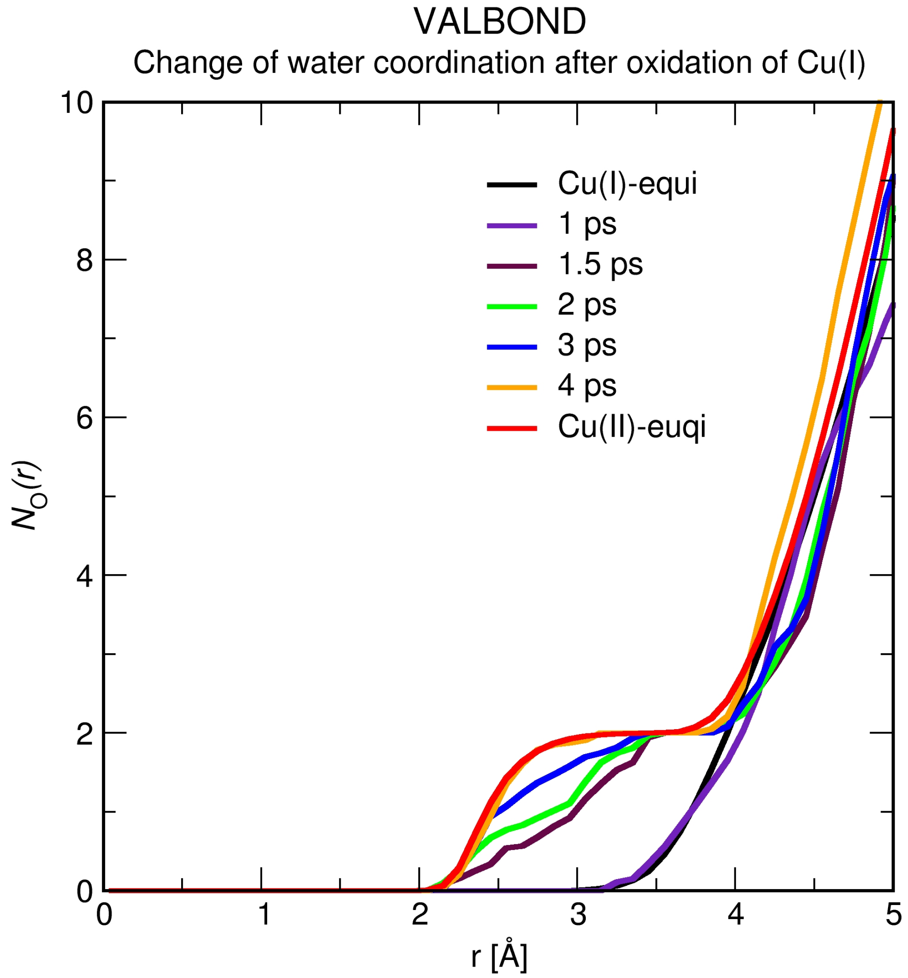

Figure 4.22.: Excitation of Cu(I)-imidazole$_4$: Oxidation of Cu(I) to Cu(II) results in a readjustment of the solvation shell. The number of water molecules coordinating the newly formed copper(II)-complex within 5 Å equals the Cu(II)-imidazole$_4$ equilibrium within 4 picoseconds after excitation. Remarkably, the solvation shell flips in a fast pace within 500 femtoseconds: 1ps (purple) after the excitation, the solvation shell equals the initial state but only 0.5 ps after (i.e. 1.5 ps line, brown) rearranges towards a two water molecule coordination.

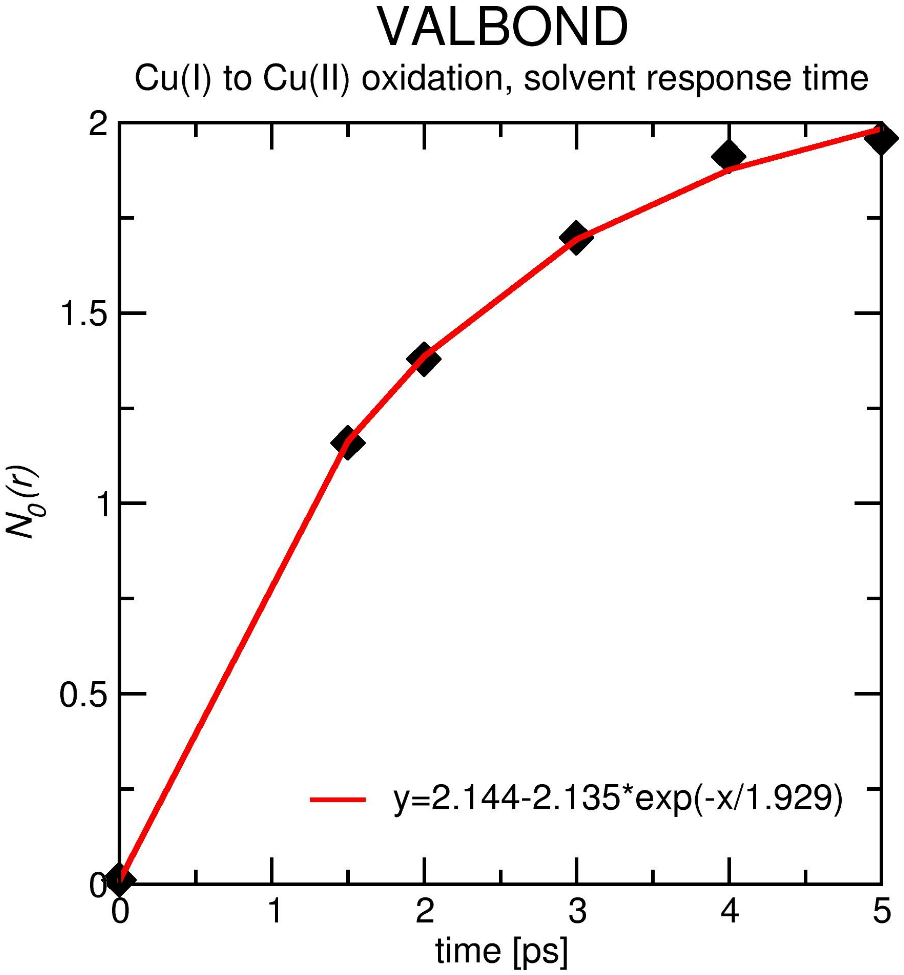

Figure 4.23.: Solvent reorganization time at 3 Å from the metal center, $\tau_{H_2O} = 1.929$ ps.

4.4. Copper(I/II)-ion parametrization of Lennard-Jones parameter

The free energy calculation was started with initial partial charges obtained by DFT B3LYP 6-31 G (d,p) calculations of a copper ion surrounded by 6 water molecules. After optimization the NBO partial charges were used during the PSF generation. During the perturbation, the charge of the copper ion was increasing to 1.237 eV from 0.649 eV for Cu^+, while the σ and ϵ parameters of the Lennard-Jones model for Van-der-Waals interaction were changed to reproduce the reported change in the free energy[40] of $\Delta F_{Cu(I)->Cu(II)} = -106^{kcal}/_{mol}$. The results are shown in figure Figure 4.24 and Table 4.5, but to draw conclusions, more calculations have to be done. While changing σ or ϵ values of one ion, all other values where kept constant at $\sigma_{Cu(I)} = 1.38\,\text{Å}$ and $\epsilon_{Cu(I)} = -0.06\,^{kcal}/_{mol}$ for copper(I) (obtained by Swissparam) and $\sigma_{Cu(II)} = 0.87\,\text{Å}$ and $\epsilon_{Cu(II)} = -0.711\,^{kcal}/_{mol}$ for copper(I) (already included in CHARMM). Using theses default parameters, a $\Delta F_{Cu(I)->Cu(II)} = -129.92^{kcal}/_{mol}$ is simulated.

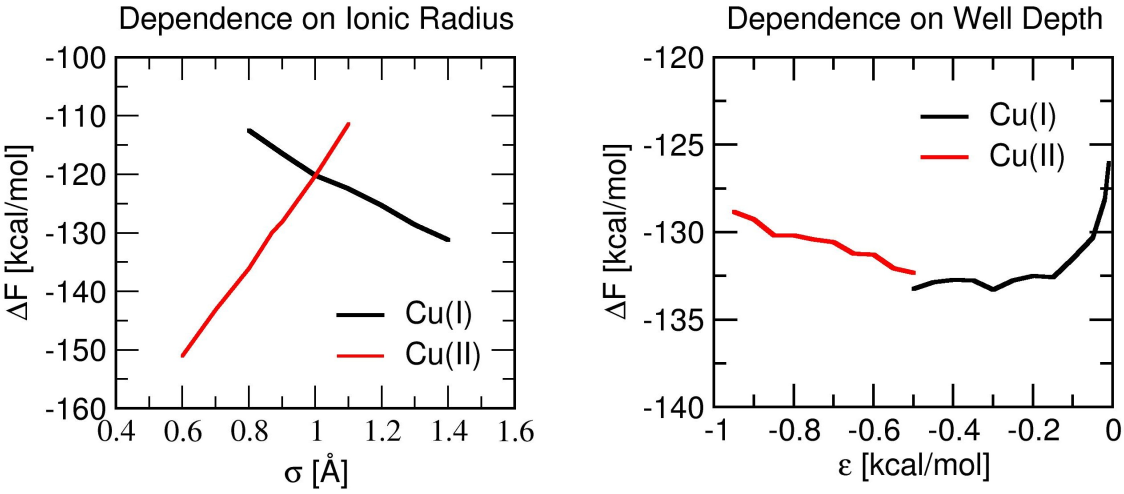

Figure 4.24.: Free energy calculation of the oxidation from Cu(I) to Cu(II). Varying the σ or ϵ values of one ion, while keeping all other values constant, resulted in the above graphs. Experimental reported $\Delta F_{Cu(I)->Cu(II)} = -106^{kcal}/_{mol}$.

Table 4.5.: Trial parameters for the Cu(I)->Cu(II) oxidation in water. Experimental value from literature[40]. The closest value is obtained using the parameters of trial C.

	$\sigma_{Cu(I)}$ Å	$\sigma_{Cu(II)}$Å	$\epsilon_{Cu(I)}$ ${}^{kcal}\!/\!{}_{mol}$	$\epsilon_{Cu(II)}$ ${}^{kcal}\!/\!{}_{mol}$	$\triangle F$ ${}^{kcal}\!/\!{}_{mol}$
Default	1.38	0.87	-0.06	-0.711	-130
A	0.77	0.73	-0.01	-0.95	-116
B	1.38	0.87	-0.01	-0.95	-125
C	1.00	0.95	-0.06	-0.711	-113
Experimental	-	-	-	-	-106

5. Conclusion

5.1. Parametrization of *trans* influence

The performed parametrization covered 10 different ligands resulting in a library of 720 structures. Due to the problems with the self consistent field (SCF) convergence and other failures 120 structures could not be investigated. Because the parametrization fit was not as good as expected, 2 ligands, namely bromide and phosphine had to be excluded, lowering the number of analyzed structures from 600 down to 266. The approach of broadening the ligand set, for example with 2-methyl-pyridine which could be anticipated to give results similar to ammonia ligands, was not a fruitful decision. Instead of inflating the number of structures by adding 2-methyl-pyridine and fluoride, a close investigation of the failed DFT calculations would have been a better path. For example the use of a bigger basis set like LANL2DZ could have solved that problem. Nevertheless, the obtained Trans parameters can be used for Valbond-Trans calculations of organometallic and metalloprotein substances. The presented findings revealed as prominent *trans* influencers alkyl, chloride and hydride ligands, weak *trans* influencers are nitrogen containing ligands, whether tested as ammonia or 2-methyl-pyridine ligand and oxygen (aqua) and sulfur (hydrogen sulfide). Inclusion of 2-methyl-pyridine did not show a big difference compared to the Trans parameters derived from ammonia, the slight differences can be attributed to steric effects of the larger 2-methyl-pyridine, see Table A.12. In agreement with previous studies, sulfur and oxygen are shown to be most sensitive whereas alkyl, hydride and fluoride are least sensitive and thus tend bound trans to them (*antisymbiosis*).[52] From the reported parameters of the structural *trans* influence of all subsets, a series depending on the ligands sensitivity and intensity can be constructed: s_A: $\mathrm{C}^{CH_3^-} < \mathrm{F}^- < \mathrm{H}^- < \mathrm{N}^{NH_3} < \mathrm{N}^{py} < \mathrm{Cl}^- < \mathrm{O}^{H_2O} < \mathrm{S}^{H_2S}$, i_B: $\mathrm{O}^{H_2O} < \mathrm{S}^{H_2S} < \mathrm{N}^{NH_3} < \mathrm{F}^- < \mathrm{N}^{py} < \mathrm{Cl}^- < \mathrm{H}^- < \mathrm{C}^{CH_3^-}$. For a study of the cystein-copper(II) interaction the derived sulfur parameters can be misleading but worth a trial. DFT calculations of a water coordinated copper(II) ion has shown an effective charge of +1.23 eV due to metal-to-ligand-charge transfer. If a square planar copper(II) complex includes of two anionic ligands, the electrostatic attracted hydrogen sulfide tend to dissociate, hence the presented sulfur parameters should be considered preliminary. As a next step, one could use the derived Valbond-Trans parameter to reproduce the bond lengths of known X-ray structures of square planar copper(II) complexes like aqua-ammine-(μ-succinato)copper(II) dihydrate[29] (WebCSD entry PUFQOX). Next, the nonbonded parameters can be adjusted as described in previous works[21].

5.2. Dynamics of Copper(I/II)-imidazole$_4$

The presented simulation comparison impresses with the good reproducibility of experimental observations by VALBOND. The solvation shell behavior was in better agreement with XAS results if NBO partial charges were assigned to the structure in VALBOND than the solvation shell behavior observed with the quantum mechanistic DFTB3 calculation. Besides, the geometrical rearrangement after oxidation could be performed by VALBOND in a sophisticated manner albeit the change happens almost instantaneously, it is worth noting that it is possible to predict at all. Although the gradually rearrangement as observed with DFTB3 could be seen as the naturally occurring one, studies of the structural change upon oxidation and/or reduction of copper(I/II) in proteins could be carried out by a CHARMM/VALBOND-TRANS force field up to 33 times faster than using a CHARMM/DFTB3 mixed force-field/QM simulation. Further gain in insight is possible in the field of dye-sensitized solar cells. Utilizing the new DFTB3 method, calculations of the geometrical change upon oxidation of the sensitizer molecule allows the screening for ligands which stay rigid, protecting the copper core from solvent attacks by $\pi-\pi$ stacking, thereby extending the excited states lifetimes, while also allows the $I^-/I^-{}_3$ electrolyte the regeneration of the dye via a push-pull model [23]. A tuning of the shielding- vs. regeneration properties could improve the photon-electron conversion efficiency for intense light conditions, if the recombination of already injected electrons in the semiconductor back to the oxidized dye can be prohibited by a tailor made sensitizer molecule (recombination occurs on the micro- to millisecond scale process[17]).

The DFTB3 calculations of copper(I)-imidazole$_4$ were observed to be more flexible at room temperature than copper(II)-imidazole$_4$. The presented thermic fluctuations of the bond length, Figure 4.18, resulted in problems with the structural integrity for longer simulations (700-900 ps), whereas even 3 ns simulations of Cu(II)-imidazole$_4$ experienced no problems. Although the $3d^9$ configuration of copper(II) is more stable that the $3d^{10}$ configurations of copper(I), the reason could be a inadequate parametrization of copper with carbon containing ligands as earlier studies with ammonia ligands were carried out without that observation[28]. To summarize, at the moment, the VALBOND method should be considered first for geometrical studies of organometallic and bio-inorganic complexes. The less computational time needed as well as the good agreement with experimental values makes the DFTB3 calculation only necessary for reactivity studies.

5.3. Free energy calculations of the copper(I) oxidation in water

The presented dependence of the free energy change for the copper(I) oxidation on the Lennard-Jones parameter should investigated more to come up with refined parameters for the van-der-Waals interactions of copper ions. In relation with the presented VALBOND-TRANS parametrization, which refined the bonded interaction, the refinement of non bonded interactions may lead to improved dynamics of copper containing system, like the discussed protein families and organometallic and bio-inorganic substances in technological applications.

Acknowledgments

I gratefully thank Prof. Meuwly and Prof. Housecroft for their great support and the opportunity to perform my thesis under their supervision. I would also like to acknowledge the outstanding assistance of Prof. Meuwly's group, namely Akshaya Kumar Das, Zhen-Hao Xu, Florent Hedin, Dr. Polydefkis Diamantis, Dr. Padmabati Mondal, Dr. Otoniel Denis-Alpizar, Dr. Krystel El Hage, Sebastian Brickel, Oliver Unke, Marco Pezzella, Dr. Shampa Raghunanthan and last but not least Dr. Michael Devereux (special thanks for waiting for me at the hiking trip). The hints you gave me as well as the instructive discussion during the last 6 month helped me to gain valuable knowledge about computational chemistry.

A. Parameters for energetic and structural trans effect

A.1. All isomers set

Table A.1.: Energetic trans effect - fitting parameters for all isomers of copper(II) square planar complexes with ligand A trans to ligand B: $\Delta U_{trans} = \sum_{trans} p_{AB}$
All values are in ${}^{kcal}/_{mol}$

p_{PH_3-Br} -2.29770	p_{PH_3-Cl} -2.30598	$p_{PH_3-NH_3}$ 1.82766	$p_{PH_3-H_2O}$ 1.51839	$p_{PH_3-CH_3}$ 1.03197	p_{PH_3-H} 0.34863
$p_{PH_3-H_2S}$ 0.63309	$p_{PH_3-N_{pyridine}}$ -0.40854	p_{PH_3-F} -1.50645	p_{Br-Cl} 0.03518	p_{Br-NH_3} 0.10007	p_{Br-H_2O} -2.48925
p_{Br-CH_3} 1.54017	p_{Br-H} 1.56206	p_{Br-H_2S} -2.12803	$p_{Br-N_{pyridine}}$ -0.54502	p_{Br-F} 0.79386	p_{Cl-NH_3} -2.64789
p_{Cl-H_2O} -4.22288	p_{Cl-CH_3} -0.11746	p_{Cl-H} 1.05447	p_{Cl-H_2S} -3.38971	$p_{Cl-N_{pyridine}}$ -1.53062	p_{Cl-F} -0.32916
$p_{NH_3-H_2O}$ 2.01050	$p_{NH_3-CH_3}$ 0.65132	p_{NH_3-H} 0.46795	$p_{NH_3-H_2S}$ 1.70549	$p_{NH_3-N_{pyridine}}$ 2.92708	p_{NH_3-F} -1.48293
$p_{H_2O-CH_3}$ 0.63701	p_{H_2O-H} -0.38908	$p_{H_2O-H_2S}$ 0.45330	$p_{H_2O-N_{pyridine}}$ 0.86250	p_{H_2O-F} -2.11572	
p_{CH_3H} -2.33959	$p_{CH_3H_2S}$ 1.85309	$p_{CH_3-N_{pyridine}}$ 1.24696	p_{CH_3-F} 1.10986		$p_{PH_3-PH_3}$ 0.57924
p_{H-H_2S} 0.65043	$p_{H-N_{pyridine}}$ -0.09647	p_{H-F} 3.12098		p_{Br-Br} 1.71440	p_{Cl-Cl} -0.58716
$p_{H_2S-N_{pyridine}}$ -0.00835	p_{H_2S-F} -4.95801		$p_{NH_3-NH_3}$ 4.64317	$p_{H_2O-H_2O}$ -1.89223	$p_{CH_3-CH_3}$ -1.54368
$p_{N_{pyridine}-F}$ -1.20531		p_{H-H} -0.60748	$p_{H_2S-H_2S}$ 2.59429	$p_{N_{pyridine}-N_{pyridine}}$ 0.87672	p_{F-F} 2.59175

Table A.2.: Fitting parameters for copper(II) ligands: bond lengthening sensitivity of ligand A s_A, of ligand B i_B, and the unperturbed copper(II) - ligand distance r_A^0 . The fitting parameters are normalized with respect to chloride.

	$r_A^0\left[\text{Å}\right]$	s_A	i_B
Cl	2.345	1.00	1.00
P_{PH_3}	2.384	2.12	0.92
Br	2.422	-2.16	1.24
N_{NH_3}	2.038	0.35	0.70
O_{H_2O}	1.939	7.00	0.52
C_{CH_3}	2.108	-5.32	2.11
H	1.626	-3.39	1.79
S_{H_2S}	2.409	8.85	0.58
$N_{pyidine}$	1.984	1.46	1.16
F	1.876	-2.57	0.98

	$\left[\text{Å}\right]$
deviation^{2}sum $\left[\text{Å}^2\right]$	43.0076
root mean square deviation	0.1398
mean absolute error	0.0840
maximum deviation	0.390
minimum deviation	-1.437

A.2. Subset 1

Table A.3.: Energetic trans effect for the subset 1 - fitting parameters for copper(II) square planar complexes with ligand A trans to ligand B: $\Delta U_{trans} = \sum_{trans} p_{AB}$ All values are in ${}^{kcal}/_{mol}$

p_{Cl-Cl} 1.95477	$p_{NH_3-NH_3}$ 1.71449	$p_{H_2O-H_2O}$ 0.01568	$p_{CH_3-CH_3}$ -1.18864	p_{H-H} -0.35820
p_{Cl-NH_3} -2.77028	p_{Cl-H_2O} -3.72124	p_{Cl-CH_3} 2.08084	p_{Cl-H} 2.73413	$p_{NH_3-H_2O}$ 0.66013
$p_{NH_3-CH_3}$ -1.41374	p_{NH_3-H} -0.89354	$p_{H_2O-CH_3}$ 1.87047	p_{H_2O-H} 0.16585	p_{CH_3-H} -0.19123

Table A.4.: Fitting parameters for copper(II) ligands of the subset 1: s_A and i_B, r_A^0 the unperturbed copper(II) - ligand distance. The fitting parameters are normalized with respect to chloride.

	$r_A^0\left[\text{Å}\right]$	s_A	i_B
Cl	2.345	1.00	1.00
N_{NH_3}	2.038	0.06	0.67
O_{H_2O}	1.939	11.92	0.35
C_{CH_3}	2.108	-4.84	1.38
H	1.626	-2.84	1.20

	$\left[\text{Å}\right]$
deviation^{2}sum$\left[\text{Å}^2\right]$	2.3345
root mean square deviation	0.1126
mean absolute error	0.0830
maximum deviation	0.234
minimum deviation	-0.610

A.3. Subset 2

Table A.5.: Energetic trans effect for the subset 2 - fitting parameters for copper(II) square planar complexes with ligand A trans to ligand B: $\Delta U_{trans} = \sum_{trans} p_{AB}$ All values are in $^{kcal}/_{mol}$

p_{Cl-Cl} 0.81318	$p_{NH_3-NH_3}$ 2.50900	$p_{H_2O-H_2O}$ 0.47455	$p_{CH_3-CH_3}$ -1.53260	p_{H-H} -0.82162	p_{F-F} 1.94329
p_{Cl-NH_3} -3.17852	p_{Cl-H_2O} -3.89835	p_{Cl-CH_3} 1.19591	p_{Cl-H} 1.49783	p_{Cl-F} 2.75678	$p_{NH_3-H_2O}$ 1.90885
$p_{NH_3-CH_3}$ -1.12869	p_{NH_3-H} -1.10525	p_{NH_3-F} -1.51461	$p_{H_2O-CH_3}$ 2.18453	p_{H_2O-H} 0.42302	p_{H_2O-F} -1.56722
p_{CH_3-H} -0.76915	p_{CH_3-F} 1.58251	p_{H-F} 1.59675			

Table A.6.: Fitting parameters for copper(II) ligands of the subset 2: s_A and i_B, r_A^0 the unperturbed copper(II) - ligand distance. The fitting parameters are normalized with respect to chloride.

	$r_A^0\,[\text{Å}]$	s_A	i_B
Cl	2.345	1.00	1.00
N_{NH_3}	2.038	0.27	0.79
O_{H_2O}	1.939	11.75	0.48
C_{CH_3}	2.108	-5.88	1.10
H	1.626	-4.26	1.08
F	1.876	-3.48	0.61

	[Å]
deviation^{2}sum $[\text{Å}^2]$	3.0256
root mean square deviation	0.0938
mean absolute error	0.0663
maximum deviation	0.237
minimum deviation	-0.678

A.4. Subset 3

Table A.7.: Energetic trans effect for the subset 3 - fitting parameters for copper(II) square planar complexes with ligand A trans to ligand B: $\Delta U_{trans} = \sum_{trans} p_{AB}$ All values are in $^{kcal}/_{mol}$

p_{Cl-Cl} 1.06665	$p_{NH_3-NH_3}$ 2.26024	$p_{H_2O-H_2O}$ -0.50902	$p_{CH_3-CH_3}$ -1.64634	p_{H-H} -0.89465	p_{F-F} 3.14224	$p_{Pyridine-Pyridine}$ 0.35556
p_{Cl-NH_3} -3.47031	p_{Cl-H_2O} -3.54830	p_{Cl-CH_3} 1.47307	p_{Cl-H} 2.44165	p_{Cl-F} 1.78423	$p_{Cl-Pyridine}$ -0.81357	$p_{NH_3-H_2O}$ 2.29148
$p_{NH_3-CH_3}$ -1.24989	p_{NH_3-H} -0.90400	p_{NH_3-F} -2.35540	$p_{NH_3-Pyridine}$ 1.16790	$p_{H_2O-CH_3}$ 1.94121	p_{H_2O-H} 0.55023	p_{H_2O-F} -2.06346
$p_{H_2O-Pyridine}$ -2.06346	p_{CH_3-H} -1.43611	p_{CH_3-F} 2.47062	$p_{CH_3-Pyridine}$ 0.09406	p_{H-F} 2.14252	$p_{H-Pyridine}$ -1.00489	$p_{Pyridine-F}$ -2.00174

Table A.8.: Fitting parameters for copper(II) ligands of the subset 3: s_A and i_B, r_A^0 the unperturbed copper(II) - ligand distance. The fitting parameters are normalized with respect to chloride.

	$r_A^0\left[\text{Å}\right]$	s_A	i_B
Cl	2.345	1.00	1.00
N_{NH_3}	2.038	0.78	0.70
O_{H_2O}	1.939	11.53	0.52
C_{CH_3}	2.108	-6.68	1.22
H	1.626	-4.80	1.13
F	1.876	-3.44	0.68
$N_{Pyridine}$	1.984	1.99	0.73

	$\left[\text{Å}\right]$
deviation^{2}sum $\left[\text{Å}^2\right]$	5.1964
root mean square deviation	0.0903
mean absolute error	0.0643
maximum deviation	0.234
minimum deviation	-0.655

A.5. Subset 4

Table A.9.: Energetic trans effect for the subset 4 - fitting parameters for copper(II) square planar complexes with ligand A trans to ligand B: $\Delta U_{trans} = \sum_{trans} p_{AB}$ All values are in ${}^{kcal}/_{mol}$

p_{Cl-Cl} 2.10109	$p_{NH_3-NH_3}$ 1.69005	$p_{H_2O-H_2O}$ -0.00869	$p_{CH_3-CH_3}$ -1.21301	p_{H-H} -0.38262	$p_{H_2S-H_2S}$ 0.80558
p_{Cl-NH_3} -2.18430	p_{Cl-H_2O} -2.66942	p_{Cl-CH_3} 1.47395	p_{Cl-H} 1.94705	p_{Cl-H_2S} -2.76934	$p_{NH_3-H_2O}$ 1.01874
$p_{NH_3-CH_3}$ -0.92449	p_{NH_3-H} -0.92531	$p_{NH_3-H_2S}$ -0.36480	$p_{H_2O-CH_3}$ 1.18052	p_{H_2O-H} -0.11099	$p_{H_2O-H_2S}$ 0.59861
p_{CH_3-H} -0.18689	$p_{CH_3-H_2S}$ 0.88300	p_{H-H_2S} 0.04134			

Table A.10.: Fitting parameters for copper(II) ligands of the subset 4: s_A and i_B, r_A^0 the unperturbed copper(II) - ligand distance. The fitting parameters are normalized with respect to chloride.

	$r_A^0\left[\text{Å}\right]$	s_A	i_B
Cl	2.345	1.00	1.00
N_{NH_3}	2.038	-0.03	0.67
O_{H_2O}	1.939	5.86	0.44
C_{CH_3}	2.108	-2.59	2.71
H	1.626	-1.29	2.42
S_{H_2S}	2.409	7.36	0.37

	$\left[\text{Å}\right]$
deviation^{2}sum $\left[\text{Å}^2\right]$	9.270
root mean square deviation	0.1616
mean absolute error	0.1067
maximum deviation	0.387
minimum deviation	-1.029

A.6. Subset 5

Table A.11.: Energetic trans effect for the subset 5 - fitting parameters for copper(II) square planar complexes with ligand A trans to ligand B: $\Delta U_{trans} = \sum_{trans} p_{AB}$
All values are in ${}^{kcal}/_{mol}$

p_{Cl-Cl} 1.78223	$p_{NH_3-NH_3}$ 1.82016	$p_{H_2O-H_2O}$ -0.84301	$p_{CH_3-CH_3}$ -1.79449	p_{H-H} -0.80899	$p_{H_2S-H_2S}$ 2.65530
$p_{Pyridine-Pyridine}$ 0.29818	p_{F-F} 3.20150	p_{Cl-NH_3} -2.75447	p_{Cl-H_2O} -2.76410	p_{Cl-CH_3} 1.25764	p_{Cl-H} 2.29338
p_{Cl-H_2S} -3.16090	$p_{Cl-Pyridine}$ -0.52710	p_{Cl-F} 2.09099	$p_{NH_3-H_2O}$ 2.05396	$p_{NH_3-CH_3}$ -1.11939	p_{NH_3-H} -1.0277
$p_{NH_3-H_2S}$ 0.66798	$p_{NH_3-Pyridine}$ 1.11829	p_{NH_3-F} -2.57900	$p_{H_2O-CH_3}$ 1.35281	p_{H_2O-H} 0.17590	$p_{H_2O-H_2S}$ 1.36932
$p_{H_2O-Pyridine}$ 1.39328	p_{H_2O-F} -1.89516	p_{CH_3-H} -1.20949	$p_{CH_3-H_2S}$ 1.11847	$p_{CH_3-Pyridine}$ -0.14738	p_{CH_3-F} 2.33646
p_{H-H_2S} 0.54465	$p_{H-Pyridine}$ -0.77073	p_{H-F} 1.61198	$p_{H_2S-Pyridine}$ 0.22794	p_{H_2S-F} -6.07808	$p_{Pyridine-F}$ -1.89064

Table A.12.: Fitting parameters for copper(II) ligands of the subset 5: s_A and i_B, r_A^0 the unperturbed copper(II) - ligand distance. The fitting parameters are normalized with respect to chloride.

	$r_A^0\left[\text{Å}\right]$	s_A	i_B
Cl	2.345	1.00	1.00
N_{NH_3}	2.038	0.75	0.51
O_{H_2O}	1.939	8.28	0.29
C_{CH_3}	2.108	-1.44	2.45
H	1.626	-0.64	1.02
S_{H_2S}	2.409	9.77	0.37
$N_{Pyridine}$	1.984	0.84	0.79
F	1.876	-0.74	0.53

	$\left[\text{Å}\right]$
deviation^{2}sum $\left[\text{Å}^2\right]$	11.0402
root mean square deviation	0.1118
mean absolute error	0.0774
maximum deviation	0.383
minimum deviation	-1.032

Bibliography

[1] Viloya S. Allured, Christine M. Kelly, and Clark R. Landis. SHAPES empirical force field: new treatment of angular potentials and its application to square-planar transition-metal complexes. *Journal of the American Chemical Society*, 113(1):1–12, February 1991.

[2] Kirsty M. Anderson and A. Guy Orpen. On the relative magnitudes of cis and trans influences in metal complexes. *Chemical Communications*, (24):2682–2683, December 2001.

[3] A. D. Becke. Density-functional exchange-energy approximation with correct asymptotic behavior. *Physical Review A*, 38(6):3098–3100, September 1988.

[4] Axel D. Becke. Density functional thermochemistry. III. The role of exact exchange. *The Journal of Chemical Physics*, 98(7):5648–5652, April 1993.

[5] M. Born and R. Oppenheimer. Zur Quantentheorie der Molekeln. *Annalen der Physik*, 389(20):457–484, January 1927.

[6] Bernard R. Brooks, Robert E. Bruccoleri, Barry D. Olafson, David J. States, S. Swaminathan, and Martin Karplus. CHARMM: A program for macromolecular energy, minimization, and dynamics calculations. *Journal of Computational Chemistry*, 4(2):187–217, June 1983.

[7] Peter Comba, Hambley W. Trevor, and Martin Bodo. *Molecular Modeling of Inorganic Compounds*. Wiley-VCH Verlag GmbH & Co. KGaA, 3rd edition edition, 2006.

[8] Christopher J Cramer. *Wiley: Essentials of Computational Chemistry: Theories and Models*. Wiley, 2nd edition edition, 2004.

[9] Clark R. Landis Daniel M. Root. Valence bond concepts applied to the molecular mechanics description of molecular shapes. 1. Application to nonhypervalent molecules of the P-block. *Journal of The American Chemical Society*, 115(10), 1993.

[10] Goezde Eskici and Paul H. Axelsen. Copper and oxidative stress in the pathogenesis of Alzheimer's disease. *Biochemistry*, 51(32):6289–6311, August 2012.

[11] Timothy K. Firman and Clark R. Landis. Valence Bond Concepts Applied to the Molecular Mechanics Description of Molecular Shapes. 4. Transition Metals with n Bonds. *Journal of the American Chemical Society*, 123(47):11728–11742, November 2001.

[12] Patrick Frank and Maurizio Benfatto. The X-ray Absorption Spectroscopic Model of the Copper(II) Imidazole Complex Ion in Liquid Aqueous Solution: A Strongly Solvated Square Pyramid. *Inorganic chemistry*, 51(4):2086–96, 2012.

[13] M. J. Frisch, G. W. Trucks, H. B. Schlegel, G. E. Scuseria, M. A. Robb, J. R. Cheeseman, G. Scalmani, V. Barone, B. Mennucci, G. A. Petersson, H. Nakatsuji, M. Caricato, X. Li, H. P. Hratchian, A. F. Izmaylov, J. Bloino, G. Zheng, J. L. Sonnenberg, M. Hada, M. Ehara, K. Toyota, R. Fukuda, J. Hasegawa, M. Ishida, T. Nakajima, Y. Honda, O. Kitao, H. Nakai, T. Vreven, J. A. Montgomery, Jr., J. E. Peralta, F. Ogliaro, M. Bearpark, J. J. Heyd, E. Brothers, K. N. Kudin, V. N. Staroverov, R. Kobayashi, J. Normand, K. Raghavachari, A. Rendell, J. C. Burant, S. S. Iyengar, J. Tomasi, M. Cossi, N. Rega, J. M. Millam, M. Klene, J. E. Knox, J. B. Cross, V. Bakken, C. Adamo, J. Jaramillo, R. Gomperts, R. E. Stratmann, O. Yazyev, A. J. Austin, R. Cammi, C. Pomelli, J. W. Ochterski, R. L. Martin, K. Morokuma, V. G. Zakrzewski, G. A. Voth, P. Salvador, J. J. Dannenberg, S. Dapprich, A. D. Daniels, A. Farkas, J. B. Foresman, J. V. Ortiz, J. Cioslowski, and D. J. Fox. Gaussian09 revision e.01. Gaussian Inc. Wallingford CT 2009.

[14] Michael Gaus, Qiang Cui, and Marcus Elstner. DFTB3: Extension of the Self-Consistent-Charge Density-Functional Tight-Binding Method (SCC-DFTB). *Journal of Chemical Theory and Computation*, 7(4):931–948, April 2011.

[15] Michael Gaus, Qiang Cui, and Marcus Elstner. Density functional tight binding: application to organic and biological molecules. *Wiley Interdisciplinary Reviews: Computational Molecular Science*, 4(1):49–61, January 2014.

[16] Michael Gaus, Haiyun Jin, Darren Demapan, Anders S. Christensen, Puja Goyal, Marcus Elstner, and Qiang Cui. DFTB3 Parametrization for Copper: The Importance of Orbital Angular Momentum Dependence of Hubbard Parameters. *Journal of Chemical Theory and Computation*, 11(9):4205–4219, September 2015.

[17] Anders Hagfeldt, Gerrit Boschloo, Licheng Sun, Lars Kloo, and Henrik Pettersson. Dye-Sensitized Solar Cells. *Chemical Reviews*, 110(11):6595–6663, November 2010.

[18] Marcus D. Hanwell, Donald E. Curtis, David C. Lonie, Tim Vandermeersch, Eva Zurek, and Geoffrey R. Hutchison. Avogadro: an advanced semantic chemical editor, visualization, and analysis platform. *Journal of Cheminformatics*, 4(1):17, August 2012.

[19] P. Jeffrey Hay and Willard R. Wadt. Ab initio effective core potentials for molecular calculations. Potentials for K to Au including the outermost core orbitals. *The Journal of Chemical Physics*, 82(1), January.

[20] Walter Heitler and Fritz London. Interaction of Neutral Atoms and Homopolar Binding According to the Quantum Mechanics. *Zeitschrift fuer Physik*, (44):455–472, June 1927.

[21] Franziska D. Hofmann, Michael Devereux, Andreas Pfaltz, and Markus Meuwly. Toward force fields for atomistic simulations of iridium-containing complexes. *Journal of Computational Chemistry*, 35(1):18–29, January 2014.

[22] Richard H. Holm, Pierre Kennepohl, and Edward I. Solomon. Structural and Functional Aspects of Metal Sites in Biology. *Chemical Reviews*, 96(7):2239–2314, November 1996.

[23] Catherine E. Housecroft and Edwin C. Constable. The emergence of copper(I)-based dye sensitized solar cells. *Chemical Society Reviews*, 44(23):8386–8398, November 2015.

[24] Catherine E Housecroft and Alan G. Sharpe. *Inorganic Chemistry.* Pearson, 4th edition edition, 2012.

[25] Jing Huang, Michael Devereux, Franziska Hofmann, and Markus Meuwly. Computational Organometallic Chemistry with Force Fields. In Olaf Wiest and Yundong Wu, editors, *Computational Organometallic Chemistry*, pages 19–46. Springer Berlin Heidelberg, 2012.

[26] W. Humphrey, A. Dalke, and K. Schulten. VMD: visual molecular dynamics. *Journal of Molecular Graphics*, 14(1):33–38, 27–28, February 1996.

[27] Tsuyoshi Inoue, Hajime Sugawara, Sawako Hamanaka, Hitomi Tsukui, Eiji Suzuki, Takamitsu Kohzuma, and Yasushi Kai. Crystal Structure Determinations of Oxidized and Reduced Plastocyanin from the Cyanobacterium Synechococcus sp. PCC 7942,. *Biochemistry*, 38(19):6063–6069, May 1999.

[28] Haiyun Jin, Goyal Puja, Akshaya Kumar Das, Michael Gaus, Markus Meuwly, and Qiang Cui. Copper oxidation/reduction in water and protein: studies with DFTB3/MM and VALBOND molecular dynamics simulations. *The Journal of Physical Chemistry B*, (in print), January 2015.

[29] Shouwen Jin, Daqi Wang, Huaru Cao1, Zhiwen Zheng1, Xiang Lvm, and Songbai Huang. Crystal structure of aqua-ammine-(μ-succinato)copper(II) dihydrate. *Zeitschrift fuer Kristallographie - New Crystal Structures*, 224(1-4):411–412, 2009.

[30] J. E. Jones. On the Determination of Molecular Fields. II. From the Equation of State of a Gas. *Proceedings of the Royal Society of London A: Mathematical, Physical and Engineering Sciences*, 106(738):463–477, October 1924.

[31] William L. Jorgensen, Jayaraman Chandrasekhar, Jeffry D. Madura, Roger W. Impey, and Michael L. Klein. Comparison of simple potential functions for simulating liquid water. *The Journal of Chemical Physics*, 79(2):926–935, July 1983.

[32] George B. Kauffman. Il'ya Il'ich Chernyaev (1893-1966) and the trans effect. *Journal of Chemical Education*, 54(2):86, February 1977.

[33] Judith P. Klinman. Mechanisms Whereby Mononuclear Copper Proteins Functionalize Organic Substrates. *Chemical Reviews*, 96(7):2541–2562, January 1996.

[34] Clark R. Landis, Thomas Cleveland, and Timothy K. Firman. Valence Bond Concepts Applied to the Molecular Mechanics Description of Molecular Shapes. 3. Applications to Transition Metal Alkyls and Hydrides. *Journal of the American Chemical Society*, 120(11):2641–2649, March 1998.

[35] Clark R. Landis, Timothy K. Firman, Daniel M. Root, and Thomas Cleveland. A Valence Bond Perspective on the Molecular Shapes of Simple Metal Alkyls and Hydrides. *Journal of the American Chemical Society*, 120(8):1842–1854, March 1998.

[36] L. S. Lasdon, A. D. Waren, A. Jain, and M. Ratner. Design and Testing of a Generalized Reduced Gradient Code for Nonlinear Programming. *ACM Transactions on Mathematical Software*, 4(1):34–50, March 1978.

[37] Chengteh Lee, Weitao Yang, and Robert G. Parr. Development of the Colle-Salvetti correlation-energy formula into a functional of the electron density. *Physical Review B*, 37(2):785–789, January 1988.

[38] Gilbert N. Lewis. The Atom And The Molecule. *Journal of the American Chemical Society*, 38(4):762–785, April 1916.

[39] Guohui Li, Xiaodong Zhang, and Qiang Cui. Free Energy Perturbation Calculations with Combined QM/MM Potentials Complications, Simplifications, and Applications to Redox Potential Calculations. *Journal of Physical Chemistry B*, 107(33):8643–8653, September 2003.

[40] David R. Lide. *CRC Handbook of Chemistry and Physics, Internet Version 2005.* CRC Press, Taylor & Francis Group, 84th edition edition, 2005.

[41] Dong-Dong Lin and Duan-Jun Xu. Synthesis and crystal structure of tetra(imidazole) copper(II) terephthalate. *Journal of Coordination Chemistry*, 58(7):605–609, May 2005.

[42] F. London. The general theory of molecular forces. *Transactions of the Faraday Society*, 33(0):8b–26, January 1937.

[43] M. Mezei and D. L. Beveridge. Free Energy Simulations. *Annals of the New York Academy of Sciences*, 482(1):1–23, December 1986.

[44] Linus. Pauling. The Nature Of The Chemical Bond. Application Of Results Obtained From The Quantum Mechanics And From A Theory Of Paramagnetic Susceptibility To The Structure Of Molecules. *Journal of the American Chemical Society*, 53(4):1367–1400, April 1931.

[45] Linus Pauling. *The Nature of the Chemical Bond: An Introduction to Modern Structural Chemistry.* The George Fisher Baker Non-Resident Lectureship in Chemistry at Cornell University. Cornell University Press, Ithaca, NY, January 1960.

[46] T. J. Penfold, S. Karlsson, G. Capano, F. A. Lima, J. Rittmann, M. Reinhard, M. H. Rittmann-Frank, O. Braem, E. Baranoff, R. Abela, I. Tavernelli, U. Rothlisberger, C. J. Milne, and M. Chergui. Solvent-Induced Luminescence Quenching: Static and Time-Resolved X-Ray Absorption Spectroscopy of a Copper(I) Phenanthroline Complex. *The Journal of Physical Chemistry A*, 117(22):4591–4601, June 2013.

[47] Eric F. Pettersen, Thomas D. Goddard, Conrad C. Huang, Gregory S. Couch, Daniel M. Greenblatt, Elaine C. Meng, and Thomas E. Ferrin. UCSF Chimera–a visualization system for exploratory research and analysis. *Journal of Computational Chemistry*, 25(13):1605–1612, October 2004.

[48] Jean-Paul Ryckaert, Giovanni Ciccotti, and Herman J. C Berendsen. Numerical integration of the cartesian equations of motion of a system with constraints: molecular dynamics of n-alkanes. *Journal of Computational Physics*, 23(3):327–341, March 1977.

[49] Gotthard Seifert and Jan-Ole Joswig. Density functional tight binding-an approximate density-functional theory method. *Wiley Interdisciplinary Reviews: Computational Molecular Science*, 2(3):456–465, May 2012.

[50] Sason S. Shaik and Phillippe C. Hiberty. *A Chemist's Guide to Valence Bond Theory*. Wiley, 1st edition edition, 2008.

[51] Clark R. Landis Thomas Cleveland. Valence Bond Concepts Applied to the Molecular Mechanics Description of Molecular Shapes. 2. Applications to Hypervalent Molecules of the P-Block. *Journal of The American Chemical Society*, 118(25), 1996.

[52] Ivan Tubert-Brohman, Maurus Schmid, and Markus Meuwly. Molecular Mechanics Force Field for Octahedral Organometallic Compounds with Inclusion of the Trans Influence. *Journal of Chemical Theory and Computation*, 5(3):530–539, March 2009.

[53] Ph Wernet, K. Kunnus, I. Josefsson, I. Rajkovic, W. Quevedo, M. Beye, S. Schreck, S. Gräbel, M. Scholz, D. Nordlund, W. Zhang, R. W. Hartsock, W. F. Schlotter, J. J. Turner, B. Kennedy, F. Hennies, F. M. F. de Groot, K. J. Gaffney, S. Techert, M. Odelius, and A. Foehlisch. Orbital-specific mapping of the ligand exchange dynamics of Fe(CO)5 in solution. *Nature*, 520(7545):78–81, April 2015.

Nomenclature

$g_O(r)$	radial distribution function of water oxygen around copper
i_B	trans influence intensity
r_A^0	unpertubed copper(II)-ligand distance
r_{VdW}	van-der-Waals radius
s_A	bond lengthening sensitivity
B3LYP	Becke, three-parameter, Lee-Yang-Parr, a hybrid functional for DFT
BOF	bond order factor
CHARMM	Chemistry at HARvard Macromolecular Mechanics, set of force fields used for molecular dynamics
CPU	central processing unit
DFT	density functional theory
DTSC	dual-topology-single-coordinate, approach for free energy calculations
MAD	mean absolute deviation
NBO	natural bond orbital
PDB	Protein Data Bank
PES	potential energy surface
RMSD	root mean square deviation
SCF	self consistent field
SHAKE	Constraint algorithm to mantain molecular geometry, often used for water molecules
TIP3P	water model with 3 interaction points at the atom positions
VMD	visual molecular dynamics, a program to visualize MD simulations
WebCSD	webapplication of the Cambridge Crystallographic Data Centre
XAS	X-ray absorption spectra

UNIVERSITÄT BASEL

PHILOSOPHISCH-NATURWISSENSCHAFTLICHE FAKULTÄT

Erklärung zur wissenschaftlichen Redlichkeit

(beinhaltet Erklärung zu Plagiat und Betrug)

Bachelorarbeit / Masterarbeit *(nicht Zutreffendes bitte streichen)*

Titel der Arbeit *(Druckschrift)*:

Energetics and Dynamics of Cu-coordinated Complexes
Using Force Fields and Density Functional Theory

Name, Vorname *(Druckschrift)*: Burzan, Niels

Matrikelnummer: 10-056-612

Hiermit erkläre ich, dass mir bei der Abfassung dieser Arbeit nur die darin angegebene Hilfe zuteil wurde und dass ich sie nur mit den in der Arbeit angegebenen Hilfsmitteln verfasst habe.

Ich habe sämtliche verwendeten Quellen erwähnt und gemäss anerkannten wissenschaftlichen Regeln zitiert.

Diese Erklärung wird ergänzt durch eine separat abgeschlossene Vereinbarung bezüglich der Veröffentlichung oder öffentlichen Zugänglichkeit dieser Arbeit.

☐ ja ☐ nein

Ort, Datum: Basel, 21.12.2015

Unterschrift: Niels Burzan

Dieses Blatt ist in die Bachelor-, resp. Masterarbeit einzufügen.